EARTH SURFACE PROCESSES AND LANDFORMS
Earth Surf. Process. Landforms **45**, 189–206 (2020)

Published online in Wiley Online Library
(wileyonlinelibrary.com) DOI: 10.1002/esp.4793

State of Science

Boundary condition control of fluvial obstacle mark formation – framework from a geoscientific perspective

Oliver Schlömer,[1]* Jürgen Herget[1] and Thomas Euler[2]
[1] Department of Geography, University of Bonn, Meckenheimer Allee 166, 53115 Bonn, Germany
[2] North Rhine-Westphalian State Agency for Nature, Environment and Consumer Protection, Auf dem Draap 25, 40221, Düsseldorf, Germany

Received 25 April 2018; Revised 6 December 2019; Accepted 10 December 2019

*Correspondence to: Oliver Schlömer, Department of Geography, University of Bonn, Meckenheimer Allee 166, 53115 Bonn, Germany. E-mail: schloem@uni-bonn.de

ESPL
Earth Surface Processes and Landforms

ABSTRACT: Obstacle marks are sedimentary bedforms, typically composed of an upstream local scour hole and a downstream sediment accumulation in the vicinity of an obstruction that is exposed to a current. However, specific morphologies are variable in fluvial, coastal and submarine environments. Although obstacle marks and the phenomenon of local scouring are subject to different scientific disciplines, the objectives of investigations are rather incoherent and no systematic framework for analysing and evaluating boundary condition control exists yet, especially concerning limited knowledge of the cause and effect relationship of obstacle mark formation at instream boulders or vegetation elements in variable environmental conditions. Thus, a parameter framework is developed which identifies a spectrum of extrinsic and intrinsic boundary conditions that control the major process dynamics of obstacle mark formation. The framework is composed of dimensionless control parameters that are separated by a hierarchical order regarding their significance for obstacle mark formation. Primary control parameters determine the geometrical scale of flow field at the obstacle, and therefore control the potential maximum size of the obstacle. Secondary control parameters affect the dynamics of the flow field in geometrical scale and limit the potential maximum size of the emerging sedimentary structure if thresholds are crossed. The framework is supposed to be a foundation for subsequent quantification and determination of thresholds by systematic laboratory studies. To elucidate this, flume-based research is presented, evaluating the influence of different flow levels at boulder-like obstacles of different shapes. The results show that obstacle mark dimensions were maximized at shallow flow depths compared to obstacle dimensions, while deep flows at submerged boulder-like obstructions caused considerably smaller obstacle marks. In interdependency with a rounded and more streamlined obstacle shape, deep flows even cause a deviation of morphology if the flow depth above an obstacle exceeds 1.6 times the obstacle's dimensions. © 2020 The Authors. Earth Surface Processes and Landforms published by John Wiley & Sons Ltd.

KEYWORDS: obstacle marks; boundary conditions; control parameters; thresholds; physical modelling

Introduction

In general, obstacle marks are morphological features formed by coherent vortex structures induced by obstacles exposed to a current (e.g. Karcz, 1968; Richardson, 1968; Allen, 1984; Paola *et al.*, 1986). Initially, the presence of an obstruction confines the approaching flow field and leads to areas of potential scouring in front and around the obstacle, as well as depositional areas in the wake of the obstacle, due to local acceleration and deceleration of flow around the obstacle. Although obstacle marks are considered here as bed features of the fluvial environment, similar morphologies are reported from the seabed at shipwreck sites (e.g. Quinn, 2006; Garlan *et al.*, 2015; Quinn and Smyth, 2017), in the aeolian environment at sandy surfaces (e.g. Leenders *et al.*, 2007; Bishop, 2011; Luo *et al.*, 2012; McKenna Neuman *et al.*, 2013) and snow (Allen, 1965; Filhol and Sturm, 2015). In the fluvial environment, numerous natural elements are capable of serving as obstacles (e.g. boulders, deadwood and vegetation elements) (Figure 1). Studies of different scientific disciplines in Earth-science lead to synonymous expressions of erosional and depositional bed features induced by obstructions, including obstacle scour mark (Dżułyński and Walton, 1965), current crescent and current shadow (Peabody, 1947; Allen, 1984), comet mark (Werner *et al.*, 1980), obstruction-formed pool (Buffington *et al.*, 2002; Hassan and Woodsmith, 2004; Comiti *et al.*, 2005) and vegetation-induced sedimentary structure (Nakayama *et al.*, 2002; Rygel *et al.*, 2004).

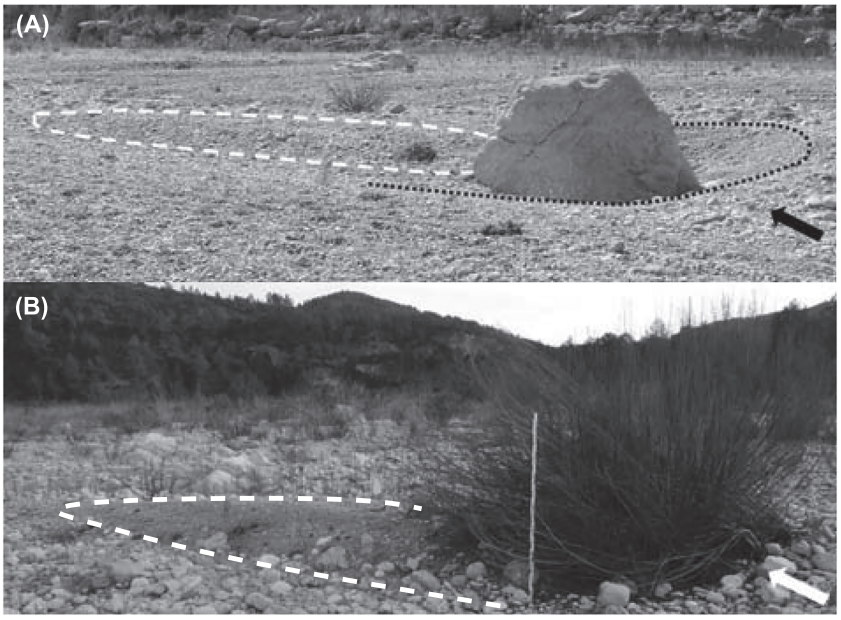

Figure 1. Sedimentary structures at obstacles in ephemeral Rambla de la Viuda, Spain. (A) Obstacle mark at a boulder (~1 m height). Black dotted line indicates upper rim of the scour hole and dashed white line indicates sediment accumulation in the wake. (B) Tapered sediment accumulation of fine gravel in the wake of an instream vegetation element. Rod (1.5 m) for scale. Arrows indicate direction of flow.

In engineering science, the expression 'local scour' is utilized to account for morphodynamic processes at man-made obstructions, such as bridge piers, river training structures and pipelines. Safety problems at these structures due to the local scour phenomenon lead to numerous physical modelling studies and deterministic approaches to evaluate the significance of various boundary conditions, including flow conditions, sediment characteristics, geometric characteristics of the obstruction and time (Breusers and Raudkivi, 1991; Hoffmans and Verheij, 1997; Melville and Coleman, 2000; Sumer and Fredsøe, 2005; Ettema *et al.*, 2011). Traditionally, the motivation of this research is to estimate the potential maximum scour depth at technical infrastructure subjected to flood events as a design parameter for foundation depth or as a proxy for risk assessment procedures (e.g. Melville and Sutherland, 1988; Chang *et al.*, 2004; Sheppard *et al.*, 2014). Most equations are derived through empirical approaches and rely on independent non-dimensional control parameters that represent boundary conditions. Naturally, these approaches do not consider specific properties of natural instream obstructions (e.g. boulders and vegetation elements) (Shamloo *et al.*, 2001; Euler and Herget, 2012; Euler *et al.*, 2017). Thus, the impact of many non-dimensional parameters on local scouring at technical infrastructure has been identified and isolated by the hydraulic engineering community, while knowledge of the boundary condition control of obstacle mark formation at natural instream obstructions is rather scarce. What is most lacking is a systematic framework that analyses obstacle marks as complex and self-organizing bedforms (e.g. Werner, 1999, 2003), not just components of it (i.e. potential maximum scour depth). In this perspective, environmental boundary conditions and derived control parameters govern the shape and dimension of the evolving bedform (Ewing and Kocurek, 2010; Kocurek *et al.*, 2010; Chojnacki *et al.*, 2019). Obstacle mark formation is interpreted as a system of interconnecting influences, which induce positive and negative feedback loops when thresholds of control parameters are crossed.

We propose a systematic parameter framework that sorts control parameters by different categories and classifies them based on two hierarchical levels. The impact of individual control parameters is quantified by critical thresholds derived from various references on the topic. In order to assess the complexity of boundary condition control on obstacle mark formation at natural instream obstructions, specific control factors are introduced that have not been considered so far.

The framework is established as a means to investigate the interplay of environmental conditions with erosional and depositional processes at obstructions within the fluvial system and to identify sensitivity by performing systematic laboratory parameter studies. It brings together knowledge from extensive literature on local scouring at artificial structures, and reveals gaps where the impact of individual control parameters is as yet inadequately explained. Besides purely academic relevance in the course of basic research on obstacle mark formation, growing knowledge of boundary condition control is supposed to be beneficial for application perspectives at field sites (cf. Figure 1).

1 Persistent obstacle marks are suitable indicators for the estimation of past local flow conditions (e.g. Herget *et al.*, 2013). However, a systematic framework of boundary condition control on obstacle mark formation can refine existing procedures to use obstacle marks as hydraulic indicators.
2 Instream solid and permeable obstacles have significant effects on structural dynamics of rivers due to sediment mobilization, sediment trapping and pioneer island formation, and are frequently used to enhance the habitat quality of degraded rivers (e.g. Radspinner *et al.*, 2010). The extent of these effects is controlled by thresholds of boundary condition, and further knowledge would be beneficial in the course of valuable and sustainable river restoration practices.

The aims of this paper are: (i) to review obstacle marks as sedimentary structures combining knowledge and experiences from different disciplines; (ii) to give a comprehensive overview of morphodynamic processes leading to the emergence of these structures; (iii) to review existing knowledge of boundary conditions and control factors of obstacle marks formation across different scientific disciplines; (iv) to sort boundary conditions and control parameters of obstacle marks formation at natural instream obstacles by different categories and hierarchies in a novel parameter framework; (v) to evaluate the effects of different water levels at the obstacle and obstacle shape on obstacle marks formation based on a laboratory flume study, to underpin the relevance of the parameter framework.

Obstacle Marks as Sedimentary Structures on Different Spatial Scales

Typically, obstacle marks are regarded as sedimentary structures that develop in non-cohesive and cohesive sediments (e.g. Briaud *et al.*, 1999; Brandimarte *et al.*, 2006; Debnath and Chaudhuri, 2010) and also in bedrock channels (e.g. Richardson and Carling, 2005; Yin *et al.*, 2016).

Obstacle marks are assembled structures, typically composed of an upstream conical depression wrapping laterally around an obstacle in the downstream direction, denoted as a scour hole, and a contiguous depositional region in the wake of the obstruction, termed a sediment ridge. The obstacle itself is considered as an integral component of the structure and consists of a large bed obstruction, typically with a diameter greater than the grain size of the surrounding alluvium (Judd and Peterson, 1969; Lisle, 1981; Thompson, 2008). The entire pattern can be characterized by certain morphometric variables characterizing length values of the scour hole, including scour depth (d_s), scour width (w_s), scour length (l_s), as well as length values of the sediment ridge (L_r), including ridge height (h_r), ridge width (w_r) and ridge length (l_r) (cf. Figure 2A) (Euler and Herget, 2012). Scour hole and sediment ridge volumes (Vol_s and Vol_r) can be estimated by multiplying the morphometric variables, although this procedure does not account for the specific shape of the structures and might lead to overestimation (Euler and Herget, 2012). The upstream scour slopes in front of the obstacle, in the plane of symmetry as well as perpendicular to it, are separable into upper and lower slope. The transition is characterized by a berm or rim as a type of 'knickpoint', which separates the steeper inner scour hole from the outer scour hole (cf. Figure 2B) (Dargahi, 1990; Hoffmans, 1993; Link *et al.*, 2008). Close to the obstacle front, a flat semi-circular scour hole is located.

Field evidence of obstacle marks at a solid obstruction has been reported on different spatial scales, resulting from overland flow at rock fragments (e.g. Poesen *et al.*, 1994), at boulders as remnants of flood events in ephemeral streams (Karcz, 1968; Euler *et al.*, 2017) and at icebergs during glacier outburst floods (jökulhlaups) (Russell, 1993; Russell *et al.*, 2006; Høgaas and Longva, 2016). Amongst the greatest obstacle marks (dimensions up to 10^2 m) are reported as evidence of Quaternary megafloods (peak discharge $> 10^6$ m^3 s^{-1}) at large boulders and bedrock hills (Baker, 1978; Baker and Bunker, 1985; Carling *et al.*, 2002b; Herget, 2005). Their macroscopic pattern is thereby consistent on different spatial scales (cf. Figure 2A). However, Nakayama (1992) describes scour holes in the wake of large boulders, while a frontal scour hole is missing. A connection can be drawn to the impact of boulders in high-gradient streams or rock sills, which are capable of inducing local scour formation in their wake due to overtopping and jet stream motion at their wake side (Buffington *et al.*, 2002; Comiti *et al.*, 2005; Endreny *et al.*, 2011; Pagliara *et al.*, 2018). However, beyond the description no further explanation based on dominant boundary conditions is available to account for this kind of 'inverse' obstacle mark.

Concerning solid instream roughness elements, like boulders in upper segments of gravel bed rivers, similar sedimentary structures – called particle clusters – are well documented as small-scale bedforms (Dal Cin, 1968; Strom and Papanicolaou, 2008; Papanicolaou and Tsakiris, 2017). Contrary to obstacle marks, no local scour hole is formed at the obstacle frontal face (stoss side). Instead, the obstacle serves as an anchor particle that traps incoming finer sediments either on its stoss side or in its wake, depending on the relative submergence ratio (i.e. ratio of flow depth to diameter of the anchor particle) of the obstructions as these bedforms evolve during the rising or falling

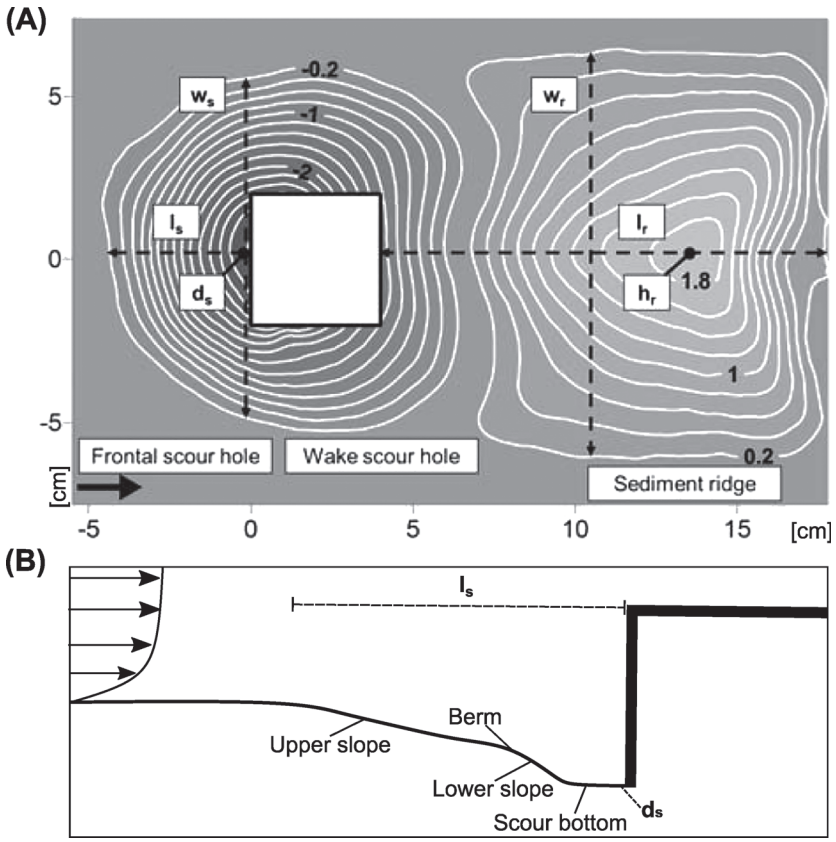

Figure 2. (A) Plan view of a typical fluvial obstacle mark at a cuboid obstacle generated in a laboratory flume. Black arrow indicates direction of flow. Scale is in centimetres. Modified after Euler and Herget (2012, p. 40). (B) Schematic upstream scour slope profile in the plane of symmetry indicating segments with different inclination, separated at a 'knickpoint' (i.e. berm). Not to scale.

limp of a hydrograph (Laronne *et al.*, 2001; Papanicolaou *et al.*, 2011, 2018; Ghilardi *et al.*, 2014b).

Obstacle marks of different spatial extent are also reported at permeable riparian vegetation elements. Rygel *et al.* (2004) introduced the expression 'vegetation-induced sedimentary structures' (VISS) to describe ancient sedimentary structures at fossil forest in floodplain strata, while Tooth and Nanson (2000), Nakayama *et al.* (2002), Rodrigues *et al.* (2007), Euler *et al.* (2014) and Corenblit *et al.* (2016) report *in-situ* evidence at grass colonies, shrubs, sprouts and mature trees. As reported by these authors, shrubs and sprouts tend to favour lee-wise deposition of sediments in their wake (i.e. sediment ridge; cf. Figures 1B and 2A), while scour holes are significantly small or even absent. On the contrary, for mature trees with a single trunk, considerable scour holes are also documented. Obstacle mark formation at individual plant scale is also investigated in laboratory studies to evaluate the impact of permeability and porosity on the flow field around vegetal elements (e.g. Chen *et al.*, 2012; Kim *et al.*, 2015; Yagci *et al.*, 2016).

Morphodynamic Processes at Instream Obstacles

Large bed obstacles exposed to a steady current are capable of modifying the flow field in their vicinity, resulting in the following processes: (1) contradiction of streamline lateral to the obstacle, causing higher flow velocities; (2) a vertical jet-like downflow towards the sediment bed at the obstacle front as a consequence of a vertical pressure gradient at the obstacle frontal face; (3) formation of a horseshoe-vortex system (HSV) at the obstacle base, resulting from the deflection of the downflow against the main flow direction; the HSV extends downstream, past the sides of the obstacle; and (4) a decelerated region of flow in the wake region of the obstacle, including a wake vortex system of detached shear layers with vertical axis of rotation (cf. Figure 3) (Allen, 1984; Dargahi, 1989; Shamloo *et al.*, 2001; Sumer, 2004; Pattenden *et al.*, 2005; Euler and Herget, 2012; Papanicolaou *et al.*, 2012; Sumner, 2013; Hajimirzaie *et al.*, 2014; Bauri and Sarkar, 2016; Launay *et al.*, 2017).

Processes (1) to (4) are capable of amplifying the bed shear stress above the critical bed shear stress for sediment mobilization, inducing local scouring in front and laterally to the obstacle, even though there is no general sediment movement in the surroundings. The main driver of sediment mobilization and local scouring is the HSV (e.g. Dargahi, 1990; Radice *et al.*, 2009; Link *et al.*, 2012; Bouratsis *et al.*, 2017). The HSV is located in the inner scour hole close to the scour hole bottom, where sediment is picked up beneath the HSV by the particle transport modes of saltation and rolling (Dey, 1996; Unger and Hager, 2007; Maity and Mazumder, 2014). The steeper inner scour hole is shaped by the HSV. The rotation of the HSV generally stabilizes the lower slope at an angle greater than the angle of repose (e.g. Hoffmans, 1993; Dey *et al.*, 1995). However, the HSV is an unsteady vortex system that randomly oscillates in time, and thereby temporarily weakens (e.g. Unger and Hager, 2007). Thus, ongoing depth incision and occasional weakening of the HSV destabilize the scour slopes and result in gravity mass movements, causing an enlargement in frontal length and width of the scour hole (cf. Figure 2). Due to the collapses, sediment grains slide into the scour bottom where they get picked up by the HSV and are transported downstream under its expanding legs as bed load. In the mid- to far-wake region the sediment gets deposited as a dune-like sediment ridge due to decreasing bed shear stress (e.g. Oliveto and Hager, 2014). Sediment transport on the sediment ridge is composed of rolling and sliding (e.g. Euler *et al.*, 2017).

Deposition of finer material in the low-energetic wake of large bed obstructions (e.g. boulders) also occurs without indication of local scouring in front of the obstruction (e.g. Thompson, 2008; Papanicolaou *et al.*, 2011, 2012). Here, fine sediments are transported as sheets or in suspension and form a tapered sediment ridge or sand shadow (Werner *et al.*, 1980) (cf. Figure 1B). However, the unique aspect about obstacle marks is that they can develop even when the threshold for general sediment movement is not exceeded (Euler and Herget, 2012). Scour depth incision is characterized by a non-linear development until an equilibrium condition is reached. The scour depth is then referred to as the equilibrium scour depth and is determined as the maximum depth of the scour hole measured from the undisturbed bed level. The equilibrium scour depth is reached asymptotically in time (cf. Figure 4).

As reported from laboratory flume studies, initial scour incision is characterized by positive feedback mechanisms due to the fact that the HSV sinks into the developing scour hole (e.g. Dey, 1996, 1999; Muzzammil and Gangadhariah, 2003; Dey and Raikar, 2007a). With ongoing temporal evolution and increasing size of the scour hole, the cross-section of the vortex increases and the shear stress under the HSV decreases as less energy per unit mass is available (e.g. Kothyari *et al.*, 1992; Mia and Nago, 2003; Li *et al.*, 2018). Thus, the feedback mechanism turns negative and dampens further evolution of scouring (Muzzammil and Gangadhariah, 2003; Muzzammil *et al.*, 2004). Once shear stress induced by the HSV is well below the critical shear stress, the equilibrium condition of scour incision is attained while gravitational movements at the upper slope also relax. If the alluvial material is non-uniform, an armour layer of coarser sediments develops at the scour hole

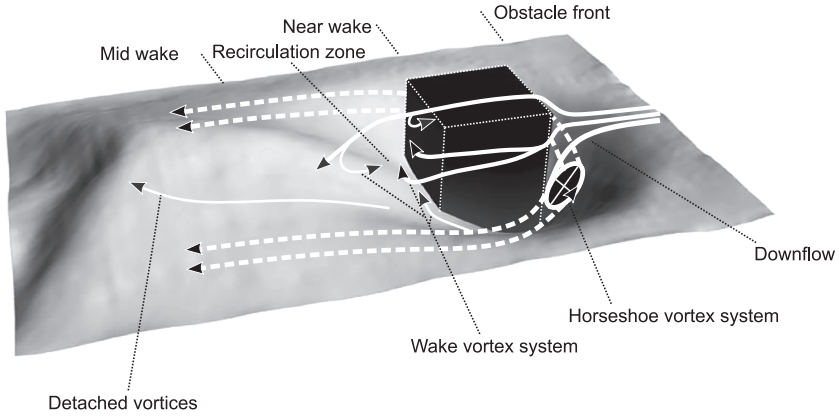

Figure 3. Schematic flow field in the vicinity of a submerged cuboid obstacle. Flow direction from right to left.

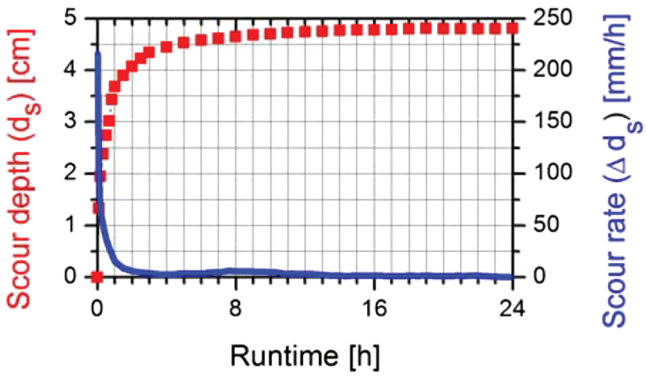

Figure 4. Temporal evolution of scour depth at a cuboid obstacle for experimental run A9. [Colour figure can be viewed at wileyonlinelibrary.com]

bottom which has a reductive impact on scour depth incision and the equilibrium condition is reached more quickly (e.g. Dey and Raikar, 2007b). From laboratory data it is known that almost 80% of equilibrium scour depth is developed within only 5–40% of the duration of experimental runs, while the time scale to reach equilibrium scour depth depends on flow conditions and sediment characteristics (Melville and Chiew, 1999).

At equilibrium conditions, the morphometric characteristics of the scour hole show a distinct relationship at which wide and long frontal scour holes belong to deeply incised scour holes, while the sediment ridge width also has a linear relationship to scour depth (Euler and Herget, 2012; Euler *et al.*, 2017). Laboratory observations indicate that feedbacks loops, resulting from dynamic interactions between hydraulic and sedimentary processes, lead to non-linear development in time towards equilibrium, although the external energy input (e.g. discharge) is constant (Euler *et al.*, 2017). This behaviour is commonly known as self-organization (e.g. Coco and Murray, 2007), and depends on the thresholds of external environmental boundary conditions as a type of cause and effect relationship (e.g. Murray *et al.*, 2014).

Review of Boundary Conditions of Morphodynamic Processes at Instream Obstructions

By referring to the advanced knowledge from hydraulic engineering science on the phenomenon of bridge pier scouring, environmental boundary conditions of local scouring are grouped into: (1) flow conditions; (2) sediment characteristics; (3) geometric characteristics of the bridge pier; and (4) time, indicating the multi-dimensional complexity of the phenomenon (e.g. Breusers and Raudkivi, 1991; Hoffmans and Verheij, 1997; Melville and Coleman, 2000; Sumer and Fredsøe, 2005; Ettema *et al.*, 2006, 2011; Williams *et al.*, 2017). Boundary conditions are composed of various influence factors that operationalize conditions (i.e. 'flow conditions') into measurable quantities (i.e. mean flow velocity and depth). Upon application of dimensional analysis and the Buckingham π-theorem (e.g. Barenblatt, 2003), these influence factors are transformed into non-dimensional, scale-invariant control parameters and displayed as functional relationships that can reasonably be analysed in physical modelling studies (e.g. Ettema *et al.*, 1998; Williams *et al.*, 2017). Local scour depth is basically controlled by flow depth (d_w; dimension L) relative to pier/obstacle width (w_o [L]), approach mean flow velocity (U_m [LT^{-1}]) relative to critical mean approach velocity for entrainment of bed sediment (U_c [LT^{-1}]), obstacle Reynolds number ($Re_o = U_m * w_o/\nu$ [$M^0L^0T^0$], with ν = kinematic viscosity [L^2T^{-1}]), obstacle Froude number ($Fr_o = U_m/g * w_o^{1/2}$ [$M^0L^0T^0$], with g = gravitational acceleration [LT^{-2}]), pier/obstacle width relative to median grain diameter (D_{50} [L]), the gradation coefficient of sediment ($\sigma_G = (D_{84}/D_{16})^{1/2}$ [$M^0L^0T^0$]), pier/obstacle shape, pier/obstacle alignment and time (t [T]) (e.g. Breusers and Raudkivi, 1991; Hoffmans and Verheij, 1997; Melville and Chiew, 1999; Melville and Coleman, 2000; Sumer and Fredsøe, 2005; Ettema *et al.*, 2011). Detailed descriptions of parameter influence – including envelope curves and empirically determined threshold – are given in the aforementioned references.

Obviously, the research of hydraulic engineers on local scouring has a technical background, as the potential failure of technical infrastructure due to local scouring is the motive to investigate the phenomenon. In this regard, the height of the obstruction is neglected as the obstruction (i.e. bridge piers) protrudes above the water surface. Thus, obstacle height (h_o [L]) is always greater than flow depth (i.e. emergent flow prevails, $d_w \leq h_o$). This perspective might be insufficient concerning natural large bed elements, like solitary boulders located at the streambed, as it neglects flow over the obstruction (i.e. submergence, $d_w \geq h_o$). Obstacle mark formation at submerged obstacles like pipelines was investigated by Dey *et al.* (2008) and Sarkar (2014) in laboratory studies, while Euler and Herget (2011) related obstacle mark formation at submerged cylinders to an adapted obstacle Reynolds number incorporating obstacle height (h_o). Euler and Herget (2011) defined the effective obstacle size (L_o) as a length value ($h_o^{2/3} w_o^{1/3}$), leading to an adapted obstacle Reynolds number ($Re_o = U_m L_o/\nu$). The exponents were chosen to account for the impact of obstacle height (h_o) on local scouring at submerged obstacles and derived from a data analysis on pier and abutment scouring reported in Oliveto and Hager (2002). Re_o expresses the ratio between turbulent and viscous stresses at the obstacle (Euler and Herget, 2011; Lança *et al.*, 2016; Manes *et al.*, 2018) and thresholds for the initiation of obstacle mark formation based on the Re_o number are formulated (Euler and Herget, 2012). The product of U_m and L_o thereby controls the turbulence and erosive energy of the HSV as it determines the flow separation and adverse pressure gradients at the obstacle frontal face (Muzzammil and Gangadhariah, 2003; Muzzammil *et al.*, 2004). However, the size of the HSV also depends on flow depth (d_w) and the structure of the approaching boundary layer (Sumer and Fredsøe, 2005; see Figure 3.3 therein). Although the flow over the obstruction ($d_w > h_o$) is a common feature at boulder-like obstacles, its implication for local scouring and obstacle mark formation has been considered in only a few empirical studies so far (Fisher and Klingeman, 1984; Shamloo *et al.*, 2001; Tominga, 2014). As opposed to this, the influence of emergent ($d_w < h_o$) and submerged ($d_w \geq h_o$) flow

has been analysed sufficiently in the course of bed load transport around large roughness elements and pebble cluster formation in gravel bed rivers, identifying the submergence ratio (d_w/h_o) as a dominant control parameter for the deposition of incoming sediments (Kramer and Papanicolaou, 2006; Papanicolaou and Kramer, 2006; Papanicolaou *et al.*, 2010; Ghilardi *et al.*, 2014a), while the boundary conditions of the surrounding alluvial bed material in relation to the diameter of the roughness element inhibit the formation of a local scour hole in front of the obstruction. Considering a solitary solid boulder-like obstruction located in a straight, moderately sloped channel with subcritical ($Fr < 1$) flow conditions and cohesion less alluvial sediment (i.e. plane bed-type streams; Simons and Richardson, 1966), local scour incision can functionally be determined by:

$$d_s = f(d_w, U_m, \rho, v, g, B, h_o, w_o, le_o, Mb, D_{50}, \rho_s, \sigma_G, U_c, d_{sed}, t) \tag{1}$$

where d_s is local scour depth [L], ρ is water density [ML^{-3}], B is channel cross-section [L], le_o is length of obstacle in streamwise direction [L], Mb is an indicator for the mobility of a boulder-like obstruction, due to tilting into the scoured depression which limits further evolution of local scouring and induces equilibrium more quickly (e.g. Truelsen *et al.*, 2005; Friedrich *et al.*, 2016; Euler *et al.*, 2017; Rennie *et al.*, 2017), ρ_s is sediment density and d_{sed} is the thickness of the alluvial layer [L].

Considering a solitary riparian vegetation element (i.e. mature tree or shrub) exposed to a current, local scouring is anticipated to be functionally determined as:

$$d_s = f\left(d_w, U_m, \rho, v, g, B, h_o, w_o, I_o, V_p, h_d, D_{50}, \rho_s, \sigma_G, U_c, d_{sed}, t\right) \tag{2}$$

where I_o is the inclination of the stem in the streamwise direction [$M^0L^0T^0$], V_p is the porosity of a permeable obstruction [$M^0L^0T^0$], which triggers bleed-flow (i.e. flow through the obstruction) instead of downflow and HSV formation (e.g. Schnauder and Moggridge, 2009) and h_d is the deflected height of a flexible vegetation element exposed to a current [L].

Equations (1) and (2) state that d_s depends on 16, respectively 17, variables (denoted n) in three basic dimensions (denoted m) that define the problem's inherent degrees of freedom (e.g. Sonin, 2004). Assuming constant relative sediment density $(\rho_s - \rho)/\rho$ (i.e. neglecting ρ and ρ_s and introducing L_o (= $h_o^{2/3} w_o^{1/3}$) as reference length) (e.g. Euler and Herget, 2011) reduces the degrees of freedom in both equations. Furthermore, application of the π-theorem (e.g. Barenblatt, 2003) to Equations (1) and (2) reveals $n - m$ non-dimensional control parameters. Among other expressions, we get:

$$d_s/L_o = f\Big(d_w/L_o, U_m/g{*}L_o{}^{1/2}\, U_m/U_c, U_m{*}L_o/v, L_o/B, Sh, Mb, L_o/D_{50}, \sigma_G, d_{sed}/L_o, t/t_e\Big) \tag{3}$$

where $U_m/g * L_o^{1/2}$ is the obstacle Froude number (Fr_o), $U_m * L_o/v$ is the obstacle Reynolds number (Re_o), L_o/B is the blockage ratio, Sh (L_o/le_o) describes the hydrodynamic shape of a body, generally differing between streamlined obstructions with cross-flow dimensions smaller than stream-wise dimensions ($Sh \leq 0.5$) and bluff obstructions with cross-flow dimensions comparable to stream-wise dimensions ($Sh \geq 0.8$) (e.g. Douglas *et al.*, 2001) and t_e is the time scale to reach equilibrium [T], which is a function of d_w/L_o, U_m/U_c and L_o/D_{50} (e.g. Melville and Chiew, 1999).

Considering a permeable vegetation element, Equation (2) can be expressed as:

$$d_s/L_o = f\big(d_w/L_o, Fr_o, U_m/U_c, Re_o, \mathrm{L_o/B}, \mathrm{I_o/I_v}, \mathrm{V_p}, \mathrm{h_d/h_o}, \mathrm{L_o/D_{50}}, \sigma_G, \mathrm{d_{sed}/L_o}, \mathrm{t/t_e}\big) \tag{4}$$

where I_v is the perpendicular alignment of the obstruction to the streambed (90°).

According to Manes and Brocchini (2015) and Manes *et al.* (2018), flow intensity (U_m/U_c) is often somewhat artificially included in the dimensional analysis of local scouring, because it has the important physical meaning of discerning between clear-water ($U_m/U_c < 1$) and live-bed conditions ($U_m/U_c > 1$) of the approaching flow (e.g. Melville and Coleman, 2000; Ettema *et al.*, 2011). For the latter, sediment mobilization is not only occurring in the vicinity of the obstruction, but also in the undisturbed flow upstream. However, as highlighted by Simarro *et al.* (2007), the usage of U_c (i.e. U_m/U_c) introduces technical difficulties in the analysis as:

$$U_c = f(D_{50}, v, g, d_w) \tag{5}$$

which can be expressed as a non-dimensional equation, applying dimensional analysis:

$$f\left(d_w/D_{50}, U_c/g{*}{D_{50}}^{1/2}, g{*}{D_{50}}^3/v^2\right) = 0 \tag{6}$$

Comparison of Equations (3), (4) and (6) indicates the analogy of several control parameters, although different reference lengths (L_o and D_{50}) are used. It becomes obvious that the control parameters d_w/L_o, Re_o and Fr_o are linked due to the consideration of U_c/U_m, because $U_m/U_c * U_c/g * D_{50}^{1/2}$ generates a derivative of Fr_o and $g * D_{50}^3/v^2$ can be rearranged to a derivative of Re_o (cf. Lança *et al.*, 2016). Thus, technically speaking, the right-hand sides of Equations (3) and (4) are not independent and one of the control parameters (i.e. d_w/L_o, Re_o or Fr_o) has to be excluded (Simarro *et al.*, 2007; Lança *et al.*, 2016). As it is preferred to keep U_m/U_c, Fr_o is excluded and the functional relationships reduce to:

$$d_s/L_o = f(d_w/L_o, U_m/U_c, Re_o, L_o/B, Sh, Mb, L_o/D_{50}, \sigma_G, d_{sed}/L_o, t/t_e) \tag{7}$$

$$d_s/L_o = f\big(d_w/L_o, U_m/U_c, Re_o, L_o/B, I_o/I_v, V_p, h_d/h_o, L_o/D_{50}, \sigma_G, d_{sed}/L_o, t/t_e\big) \tag{8}$$

Furthermore, due to shape similitude of the local scour hole (e.g. Euler and Herget, 2012), it is possible to replace d_s/L_o in Equations (5) and (6) by any characteristic length of the scour hole (cf. Figure 2A):

$$w_s/L_o \text{ and } l_s/L_o = f(d_w/L_o, U_m/U_c, Re_o, L_o/B, I_o/I_v, Sh, Mb, L_o/D_{50}, \sigma_G, d_{sed}/L_o, t/t_e) \tag{9}$$

$$w_s/L_o \text{ and } l_s/L_o = f\big(d_w/L_o, U_m/U_c, Re_o, L_o/B, I_o/I_v, V_p, h_d/h_o, L_o/D_{50}, \sigma_G, d_{sed}/L_o, t/t_e\big) \tag{10}$$

By comparing Equations (7), (8) and (9), (10), d_s/L_o can substitute any of the non-dimensional parameters on the right side

of Equations (5) and (6) (cf. Chreties *et al.*, 2008), underlining the dependence of scour depth incision for the evolution of the scour hole width (w_s) and length (l_s), besides other control parameters.

Equations (7) and (8) compromise the control parameters of obstacle mark formation at natural obstructions by including well-known parameters from hydraulic engineering research on the topic, as well as parameters that account for specific properties and characteristics of natural obstacles. However, technical considerations reveal that control parameters d_w/L_o and U_m/U_c in Equations (7) and (8) are connected due to the variables d_w and U_c [cf. Equation (5)]. Thus, a variation of one control parameter along an axis of influence often causes the variation of another parameter, which then affects the morphodynamic processes and size of the emerging obstacle mark (Ettema *et al.*, 2011).

A further systematization of the control parameters included in Equations (7) and (8) is proposed, which classifies the control parameters based on two different hierarchical levels and quantifies their impact for obstacle mark formation and size of the emerging structure based on thresholds.

Parameter Framework of Boundary Condition Control on Morphodynamic Processes at Natural Instream Obstacles

Obstacle marks are complex geomorphic systems (e.g. Werner, 1999, 2003), characterized by feedback loops of hydraulic and sedimentary processes and showing a non-linear evolution in time towards the equilibrium condition. More specifically, this behaviour is commonly known as self-organization (e.g. Coco and Murray, 2007), which depends on the thresholds of control parameters. It is supposed that the impact of control parameters on obstacle mark formation and dynamics can be assessed by thresholds of two different categories: (1) control parameters that have to be crossed to initiate local scouring and (2) control parameters that mark conditions at which obstacle marks are spatially maximized. Consequently, between these thresholds of control parameters, the size of the obstacle and its characteristic morphometric variables (cf. Figure 2A) is reduced compared to the potential maximum. From this perspective, the control factors of Equations (7) and (8) can be classified into hierarchical levels regarding their significance for obstacle mark formation and size of the emerging structure, while interconnections are also considered by this procedure.

Therefore, the 'typical' obstacle mark pattern emerging form the erosive action of the HSV and scour depth incision serves as a target of the parameter framework. Here, the control factors are grouped into extrinsic and intrinsic categories and further distinguished into levels of effectuality, including (1) hierarchy and (2) impact. Figure 5 depicts a graphical scheme that compactly demonstrates dimensional influence factors and non-dimensional control parameters of obstacle mark formation at natural instream obstacles, which are further outlined in detail.

Categories

Control parameters are separated into intrinsic and extrinsic categories. Extrinsic control parameters cluster the hydraulic conditions and alluvial characteristics as well as time, while intrinsic control parameters characterize properties of the obstacle such as geometrically definable roughness element and integral component of the emerging obstacle mark. Regarding natural instream obstacles, characteristics of solid obstacles (i.e. boulder-like) and permeable obstacles (i.e. vegetation

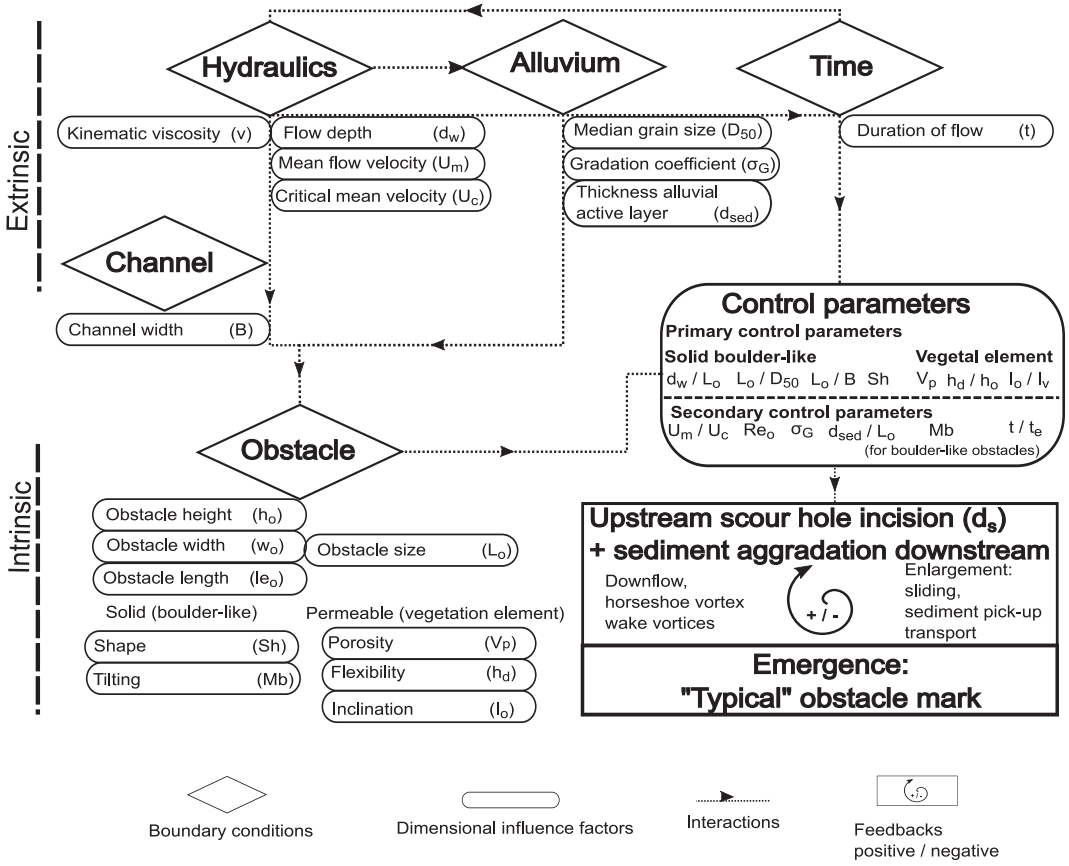

Figure 5. Block chart on boundary condition control of obstacle mark formation at natural instream obstacles. Note that the equilibrium time (t_e) is a function of d_w/L_o, U_m/U_c and L_o/D_{50} and is not displayed.

elements) are distinguished (cf. Figure 5). For solid boulder-like obstructions, *Sh* and *Mb* belong to the intrinsic control parameters. Here, bluff obstructions ($Sh \geq 0.8$) offer higher resistance to the approaching flow and generate higher-pressure gradients at the obstacle frontal face, which results in a stronger HSV and more intense local scouring processes. Boulder-like obstructions are also mobile (*Mb*). In the course of high-energy flows (i.e. $Fr \geq 1$), this might result in the mobilization of the obstacle itself and transport downstream (Carling *et al.*, 2002a; Alexander and Cooker, 2016; Bressan *et al.*, 2018). In the course of obstacle mark formation, the mobile obstacle is not transported downstream, but tilts into the evolving scour hole, if a critical scour depth is reached. This self-burial limits further scour incision and induces equilibrium more quickly (e.g. Euler *et al.*, 2017).

In contrast, shrubs are permeable obstacles. The porosity of the frontal area leads to flow penetrating the obstruction irrespective of water level (i.e. emergent or submerged) (Lee *et al.*, 2018). Vegetation porosity (V_p) represents the fraction of void spaces in relation to the total body volume and is commonly expressed as a dimensionless quantity between 0 and 1 (e.g. Grant and Nickling, 1998; Montakhab *et al.*, 2013). Indeed, porosity is not a fixed value as it depends on number and size of stems and leaves per unit area, which vary during the annual growth cycle due to exfoliation (e.g. Schnauder and Moggridge, 2009). If the obstacle is too porous, frontal scouring is inhibited due to absent downflow. Nevertheless, sediment trapping of incoming sediments is still observable (e.g. Leenders *et al.*, 2007) (cf. Figure 1B). No systematic investigation on the influence of V_p as intrinsic control parameter of obstacle mark formation has been conducted so far. Additionally, the stems and leaves of shrubs are flexible and tend to bend in a stream-wise direction as a reaction to flow passing over or through (e.g. Nikora *et al.*, 2008; Nikora, 2010). According to Okamoto and Nezu (2010), the deflected height (h_d) is an appropriate measure of the flexibility, which is primarily dependent on the rigidity of the vegetation element. The rigidity of a vegetation element determines the extent to which it offers resistance to the flow, generating pressure drag to induce local scour incision (e.g. Nikora, 2010). Thus, if the deflected height (h_d) in relation to the obstacle height (h_o) (without bending) exceeds a critical threshold, local scouring is inhibited, while again trapping of incoming sediments might still be possible (e.g. Nikora, 2010). Again, no critical threshold of h_d/h_o is formulated so far. However, the impact of inclination in a stream-wise direction (I_o) is similar to the deflected height (h_d), which is described for tree trunks of matured riparian vegetation due to local scouring (e.g. Nakayama *et al.*, 2002).

Hierarchy

Intrinsic and extrinsic control parameters are distinguished by two hierarchical levels, regarding their significance for the size of the morphometric parameters. The hierarchical levels consider connections of control parameters depicted in Equations (7) and (8).

Primary control parameters define the geometrical scale of the HSV at the obstacle and determine the potential maximum size of the morphometric variables (e.g. scour depth; cf. Figure 2A). It is supposed that the size of an obstacle mark is maximized at distinct values or within small ranges of the primary control parameters that can be interpreted as thresholds. From these thresholds, an increase or decrease of a primary control factor affects the geometrical scale of the HSV and limits the spatial extent of an obstacle mark (expressed due to the size of the morphometric variables). For given primary control parameters, the actual size of the morphometric variable is further impacted by the secondary control parameters as they influence the dynamics of the flow field at the obstacle. Generally, they characterize limitations of scour hole incision and sediment ridge accumulation and limit the potential maximum obstacle mark size below or beyond a distinct threshold (cf. Ettema *et al.*, 2011).

The control parameters L_o/D_{50}, L_o/B, d_w/L_o and *Sh* are considered as primary control parameters for obstacle mark formation at solid boulder-like obstructions, as they affect the geometrical scale of the HSV at the obstacle, while for vegetation elements porosity (V_p), relative inclination of the stem in the streamwise direction (I_o/I_v) and relative defected height of the flexible parts (h_d/h_o) are additional primary control parameters.

Within the geometrical scale, the control parameters U_m/U_c, Re_o, σ_G, d_{sed}/L_o, t/t_e and *Mb* (only for solid boulder-like obstructions) are considered as secondary control parameters which, above or below certain thresholds, impact the potential maximum size of the morphometric variables for given primary control parameters (see next section).

Impact

The impact of primary and secondary control parameters on the size of the morphometric variables is quantified by thresholds, differing conditions for which morphometric variables are potentially maximized, conditions for which morphometric variables are limited compared to a potential maximum and conditions for which obstacle mark formation is even completely inhibited. As a synthesis, these thresholds are gathered from empirical evidence reported in various references on local scouring, while scour depth (d_s) is chosen as target morphometric variable. Table I gives a comprehensive overview of known threshold ranges of primary and secondary control parameters used for the present framework, which can be summarized as follows.

1 *Relative coarseness* (D_{50}/w_o or D_{50}/L_o): d_s is maximized for relative coarseness $w_o/D_{50} \approx 25$–50 (Lee and Sturm, 2009). For $w_o/D_{50} > 60$–$10\,000$, d_s is reduced, because in non-cohesive alluvial sediment, ripple formation at the sub-threshold condition of motion ($U_m/U_c < 1$) can cause sediment transport into the scour hole. If $w_o/D_{50} < 8$, alluvial sediment particles are too coarse compared to the obstacle size and inhibit local scouring completely, because of the dissipating effects of large sediment particles on the HSV (e.g. Firat and Gungor, 2009). Under these conditions, it is more likely that the obstacle serves as an anchor particle for the formation of pebble clusters if $U_m/U_c > 1$. For the framework, w_o is replaced by L_o.
2 *Blockage ratio* (w_o/B or L_o/B): for $L_o/B < 0.1$, blockage effects on the size of d_s are negligible (e.g. Wu and Balachandar, 2016), while for increasing blockage (i.e. $L_o/B > 0.15$), d_s scales with the blockage ratio (e.g. Mazumder *et al.*, 2011). However, it is crucial to determine a threshold at which d_s is maximized. Nevertheless, Chou and Chao (2000) reported that for $L_o/B > 0.6$, no connected HSV persists in front of the obstacle as the HSV branches into several smaller vortices at the lateral edges of the obstruction.
3 *Shape* (*Sh*): d_s is maximized at bluff obstructions for $Sh \geq 0.8$, while for more streamlined obstructions ($Sh \leq 0.6$) limitations of d_s are documented (Euler *et al.*, 2017). For $Sh \leq 0.4$ the formation of an HSV and frontal scouring is supposed to ease completely.

Table I. Primary and secondary control parameters of obstacle mark formation at solid and permeable instream obstructions

Primary parameter	Maximization of d_s/L_o	Limitation of d_s/L_o	No scouring	References
d_w/L_o	0.8–1	$0.7 < d_w/L_o > 1.1$	>1.6 (for $Sh \leq 0.6$)	Within this contribution
L_o/D_{50}	~25–50	$20 < L_o/D_{50} > 60$–10 000	<8	Lee and Sturm (2009), Melville and Coleman (2000)
L_o/B	>0.15	<0.1	≥0.6	Chou and Chao (2000), Wu and Balachandar (2016)
Sh	≥0.8	≤0.6	≤0.4	Within this contribution
I_o/I_v	1	≥1.3	>>1.3	Euler *et al.* (2014)
V_p	0	?	?	—
h_d/h_o	0	?	?	—
Secondary parameter	Upper envelope	Limitation of d_s/L_o	Lower envelope	
U_m/U_c	1	>1	<0.3	Chiew (1995), Simarro *et al.* (2007)
Re_o	>4500	<4500	≤3000	Euler and Herget (2012), Manes and Brocchini (2015)
σ_G	<1.3	>1.3	if $D_{84}/L_o < 8$	Raudkivi and Ettema (1985)
Mb	—	if $d_s/l_{eo} > 0.6$	—	Euler *et al.* (2017)
d_{sed}/L_o	>1	<1	0[a]	Schloemer and Herget (2016)
t/t_e	1	<1	—	Melville and Chiew (1999)

[a] Local scouring is reported in bedrock channel (Richardson and Carling, 2005; Yin *et al.*, 2016), but not as sedimentary structure.

4 *Relative inclination of the stem in the streamwise direction* (I_o/I_v): d_s is maximized if $I_o/I_v = 1$, so that the obstacle is vertically aligned with the streambed. For $I_o/I_v \geq 1.3$, the HSV ceases to prevail due to the inclination in the streamwise direction (Euler *et al.*, 2014). Here, wake vortices create a zone of recirculating currents in the obstacle wake, causing scouring in the wake as a type of 'inverse' obstacle mark. For $I_o/I_v >> 1.3$, no frontal scour hole will emerge.

5 *Porosity* (V_p): d_s is supposed to be maximized if $V_p = 0$, so that no bleed-flow occurs. Unfortunately, there is neither empirical data available nor thresholds of $V_p > 0$ formulated that limit d_s.

6 *Relative defected height of flexible parts* (h_d/h_o): no thresholds have been described so far.

7 *Flow intensity* (U_m/U_c): for $U_m/U_c > 1$, d_s is reduced due to the passage of bedforms like ripples or dunes (e.g. Melville and Coleman, 2000; Hong *et al.*, 2017). For $U_m/U_c \leq 0.3$, no local scouring is initiated at the obstacle front, irrespective of flow depth (d_w) and obstacle size (L_o) (Chiew, 1995).

8 *Obstacle Reynolds number* (Re_o): for $Re_o < 3000$, viscous stresses dominated at the obstacle that inhibit the formation of an HSV and the emergence of a frontal scour hole, irrespective of flow depth (d_w) and obstacle size (L_o) (Euler and Herget, 2012).

9 *Gradation coefficient* (σ_G): for $\sigma_G > 1.3$ and non-uniform alluvial sediment, d_s is limited (e.g. Raudkivi and Ettema, 1985). Frontal scouring is supposed to be prevented if $D_{84}/L_o < 8$. As reported by Sheppard and Miller (2006), d_s is largely independent of σ_G at live-bed conditions ($U_m/U_c > 1$).

10 *Mobility* (Mb): if an obstacle is considered mobile, local scouring can undermine the obstacle and result in a tilting into the scour hole that will limit further d_s incision. Cleary, the tilting of a mobile obstacle depends on d_s, so that the designation of distinct thresholds is crucial. Nevertheless, Euler *et al.* (2017) experimentally determined the onset of tilting at $d_s/le_o > 0.6$.

11 *Relative sediment thickness* (d_{sed}/L_o): if an obstacle is located in a thin alluvial sediment layer above bedrock (i.e. $d_{sed}/L_o < 1$) (e.g. Hodge *et al.*, 2011; Church and Haschenburger, 2017), d_s incision is significantly limited, while slight enlargement of w_s and l_s could be observed (Schlömer and Herget, 2016). If $d_{sed}/L_o = 0$, the formation of obstacle marks as a sedimentary structure is inhibited.

12 *Time scale* (t/t_e): d_s is potentially maximized at equilibrium conditions ($t/t_e = 1$). From laboratory studies on bridge piers it is known that t_e is reached after several days, depending on flow conditions and sediment characteristics (e.g. Melville and Chiew, 1999). Scour depth (d_s) will not reach equilibrium if $t/t_e < 1$.

13 *Submergence ratio* (d_w/L_o): d_w/L_o is considered as a primary control factor and thresholds are quantified via a laboratory study hereinafter.

Evaluation of Submergence Ratio and Obstacle Shape as Primary Control Factors of Obstacle Mark Formation at Solid Boulder-Like Obstacles

Submergence ratio (d_w/L_o) and obstacle shape (Sh) are considered as primary control parameters defining the geometrical scale of the HSV, because they control the adverse pressure gradients formed at the obstacle frontal face and determine the potential maximum size of the obstacle mark. Considering a solid boulder-like instream obstruction, the variable d_w is the key determinant to attain varying ratios of d_w/L_o, as the height and width (i.e. $L_o = h_o^{2/3} w_o^{1/3}$) of the boulder-like obstruction are not supposed to change during a flood event (Lacey and Rennie, 2012). This perspective is in contrast to prior investigations on local scouring at submerged structures, where different ratios of d_w/L_o were modelled by changing the obstruction height (h_o) of a cylinder protruding into flow, keeping the flow depth (d_w) constant (e.g. Dey *et al.*, 2008; Sarkar, 2014). This caused relatively slender obstructions ($h_o > w_o$) at relatively shallow submergence ($d_w \approx h_o$), while obstacles were relatively squat ($h_o \leq w_o$) at fully submerged conditions ($d_w > h_o$).

Therefore, to quantitatively describe d_w/L_o as the primary control parameter of obstacle mark formation, a flume study is presented, in which d_w/L_o was varied by changing the approach flow depth (d_w). Three solid obstacles with nearly identical size ($h_o = 0.037$–0.04 m and $w_o = 0.04$–0.045 m, i.e. $L_o = 0.036$ to 0.037 m), but different shape (Sh) [glass cube ($Sh \geq 0.8$), glass sphere ($Sh \leq 0.6$) and elliptical sandstone pebble ($Sh \leq 0.4$)] were used to mimic boulder-like obstruction. The aim of the study was to identify the threshold condition of d_w/L_o at which obstacle marks are maximized.

Experiments were conducted in a 5-m long, 0.32-m wide and 0.27-m deep rectangular flume with fixed slope ($0.003\ \mathrm{m\,m^{-1}}$), filled with a 0.055-m thick layer of uniform medium-grained sand ($\sigma_G < 1.3$, $D_{50} = 5.5 \times 10^{-4}$ m).

In a first set of experiments (series A), individual experiments were designed to represent steady flow conditions at constant mean approach velocity ($U_m = 0.2\ m\ s^{-1}$), whereas d_w was varied from 0.02 to 0.14 m for individual runs in different intervals (0.005 to 0.02 m) by adjustment of a tail-gate at the end of the flume. The procedure resulted in submergence ratios (d_w/L_o) ranging from 0.55 to 3.83, indicating emergent conditions (obstacle's top protruded the water surface, $d_w < L_o$) to fully submerged conditions ($d_w >> L_o$) to mimic natural conditions at instream boulders adequately.

Flow depth (d_w) in the working section (~2.7 m downstream of the inlet) was measured by punctual measurements of the water surface profile along the plane of symmetry by an ultrasonic distance meter (Mic +25, Microsonic®, accuracy ±0.1 mm). By applying the principles of continuity ($Q = U_m * B$), different discharges (Q) were calculated that ensure constant U_m at different d_w based on the fixed cross-section of the flume (B). Water flux was provided by a recirculating pump (Lowara FCE-series®) and discharge was measured by a magnetic/inductive discharge meter (Schwing MS 1000®, accuracy ±1%).

For a given D_{50}, varying d_w while keeping U_m constant impacts the shear velocity (u^* [LT^{-1}]) at the undisturbed bed, which can be explained by Keugelan's resistance law for dynamical rough beds (e.g. Muste, 2017):

$$U_m/u* = 2.5 \ln(11 d_w/D_{50}) \tag{11}$$

Here, u^* decreases with rising d_w, if U_m is kept constant (e.g. Breusers and Raudkivi, 1991). Recalling Equation (5) and the interdependence of hydraulic control parameters, a variation of d_w for a given D_{50} yields different U_c:

$$U_c/u_c* = 5.75 \log(5.53 d_w/D_{50}) \tag{12}$$

for which u_c^* is the critical shear velocity [LT^{-1}] that can be estimated by a procedure given by Melville and Coleman (2000, p. 194):

$$u_c* = 0.0115 + 0.0125\, D_{50}{}^{1.4} \text{ (valid for } 0.1\ mm < D_{50} < 1\ mm) \tag{13}$$

so that:

$$U_c = 5.75 \log(5.53 d_w/D_{50}) * u_c* \tag{14}$$

By applying Equations (13) and (14) to the conditions of series A experiments, it becomes obvious that the secondary control parameter U_m/U_c was varied for different submergence ratios (d_w/L_o), ranging from 0.65 (for $d_w/L_o = 3.83$) to 0.89 (for $d_w/L_o = 0.55$), which could have been compensated by changing the slope of the flume. Unfortunately, changing the slope is not possible at the flume used.

Nevertheless, recalling the underlying assumptions of the parameter framework, d_w/L_o controls the potential maximum size of the morphometric variables as it determines the geometrical scale of the HSV, while the secondary control parameter U_m/U_c controls the dynamics of the HSV within that geometrical scale and affects the actual size of the morphometric variables.

Series A experiments were designed to determine the threshold conditions of d_w/L_o at which morphometric variables are maximized and analyse implications for the size of the morphometric variable below or beyond this threshold condition. In the present investigation, morphometric variables of the scour hole (cf. Figure 2A) and its simplified volume $Vol_s = d_s * w_s * l_s$ were analysed, normalized by $Vol_s^{1/3}/L_o$.

Series B experiments were repeated on the cuboid obstacle ($Sh \geq 0.8$) for the same ratios of d_w/L_o, keeping U_m/U_c constant ($U_m/U_c = 0.72$). From this, the observed thresholds of series A experiments are evaluated. In order to keep U_m/U_c constant at different flow depths (d_w), U_m had to be varied (0.162–0.22 $m\ s^{-1}$). This procedure also affected the secondary control parameter Re_o, which was varied for different ratios of d_w/L_o, ranging from 5928 (at $d_w/L_o = 0.55$) to 8050 (at $d_w/L_o = 3.83$).

For the present investigation, the following primary and secondary control parameters were constant: $L_o/D_{50} = 66.5$, $L_o/B = 0.11$, $\sigma_G < 1.3$, $d_{sed}/L_o > 1$, $t/t_e \geq 1$ and Mb is neglected, thus Equation (7) reduces to:

$$d_s/L_o = f(d_w/L_o, U_m/U_c, Sh) \tag{15}$$

for series A and

$$d_s/L_o = f(d_w/L_o, Re_o) \tag{16}$$

for series B.

Table II lists conditions and results of all 44 experimental runs (series A and B). The obstacles were placed in the test section of the flume (~2.7 m downstream of the inlet) in the plane of symmetry to minimize sidewall effects (e.g. Nezu and Nakagawa, 1993). Obstacles were buried 0.005 m deep in the sediment layer and mounted on a plate attached to the flume bottom to prevent tilting. The elliptical sandstone pebble was aligned with its longest axis parallel to the flow direction. For most experiments, one-dimensional vertical velocity profiles of the undisturbed approaching boundary layer were measured 0.10 m upstream of the obstacle using a miniature velocity probe (Streamflow 403, Nixon Flowmeter®, accuracy ±1.5%) to ensure the boundary layer was fully developed in the test section and followed a logarithmic distribution. Especially for low water depth (0.02–0.04 m), this procedure was not feasible, nevertheless discharge was recorded continuously by a magnetic/inductive discharge meter. During selected runs at fully submerged conditions (i.e. flow depth 0.12 m), a downlooking acoustic Doppler velocimeter (ADV) (Vectrino, Nortek AS®, accuracy ±1%) was used to measure three-dimensional velocities and turbulences in the vicinity of the obstacles along two-dimensional profiles in the plane of symmetry. The sampling frequency was 25 Hz and the flow velocity and turbulence were sampled for 60–90 s at each measuring point. Intervals in the longitudinal direction were 0.01–0.05 m, and 0.005–0.01 m in the vertical direction. Data were collected near to the end of each experimental run (>22 h) and raw data were post-processed using WinADV (Version 2.031) (Wahl, 2000), applying a spike removing and a correlation filter (e.g. Goring and Nikora, 2002; Chanson *et al.*, 2008). For the calculation of shear stress, the turbulent kinetic energy method (TKE) (e.g. Kim *et al.*, 2000; Biron *et al.*, 2004) was used, considering variances of the streamwise, cross-channel and vertical components of flow. In order to ensure obstacle marks are near equilibrium (cf. Figure 4), a runtime of 24 h was chosen (cf. Melville and Chiew, 1999). After 24 h the flume was drained and the characteristic morphometric variables of the obstacle mark were measured with point measurements of a laser distance meter (ODAM S14C, Baumer Electric®, accuracy ±1.5 mm) mounted on a carriage on top of the flume.

Table II. Boundary conditions of experiments and results

Run	Series	Type	h_o	w_o	L_o	d_w	U_m	U_c	Re_o	d_s	w_s	l_s	Vol_s
1	A	C	0.035	0.04	0.037	0.14	0.20	0.306	7319	0.022	0.105	0.04	9.24×10^{-5}
2	A	C	0.035	0.04	0.037	0.12	0.20	0.3	7319	0.023	0.108	0.049	1.22×10^{-4}
3	A	C	0.035	0.04	0.037	0.10	0.20	0.292	7319	0.026	0.113	0.052	1.53×10^{-4}
4	A	C	0.035	0.04	0.037	0.08	0.20	0.283	7319	0.031	0.137	0.066	2.8×10^{-4}
5	A	C	0.035	0.04	0.037	0.06	0.20	0.27	7319	0.042	0.182	0.078	5.96×10^{-4}
6	A	C	0.035	0.04	0.037	0.05	0.20	0.263	7319	0.038	0.173	0.077	5.06×10^{-4}
7	A	C	0.035	0.04	0.037	0.04	0.20	0.253	7319	0.047	0.189	0.075	6.66×10^{-4}
8	A	C	0.035	0.04	0.037	0.035	0.20	0.248	7319	0.047	0.195	0.081	7.42×10^{-4}
9	A	C	0.035	0.04	0.037	0.03	0.20	0.241	7319	0.047	0.193	0.082	7.44×10^{-4}
10	A	C	0.035	0.04	0.037	0.025	0.20	0.233	7319	0.047	0.192	0.079	7.13×10^{-4}
11	A	C	0.035	0.04	0.037	0.02	0.20	0.224	7319	0.042	0.181	0.075	5.7×10^{-4}
12	A	Sp	0.035	0.04	0.037	0.14	0.20	0.306	7319	0.01[a]	0.109[a]	0.06[a]	6.54×10^{-5}
13	A	Sp	0.035	0.04	0.037	0.12	0.20	0.3	7319	0.009[a]	0.107[a]	0.064[a]	6.16×10^{-4}
14	A	Sp	0.035	0.04	0.037	0.10	0.20	0.292	7319	0.009[a]	0.102[a]	0.065[a]	5.97×10^{-5}
15	A	Sp	0.035	0.04	0.037	0.08	0.20	0.283	7319	0.008[a]	0.12[a]	0.065[a]	$6{,}24 \times 10^{-5}$
16	A	Sp	0.035	0.04	0.037	0.06	0.20	0.27	7319	0.009[a]	0.126[a]	0.085[a]	9.64×10^{-5}
17	A	Sp	0.035	0.04	0.037	0.05	0.20	0.263	7319	0.002	0.03	0.004	2.4×10^{-7}
18	A	Sp	0.035	0.04	0.037	0.04	0.20	0.253	7319	0.002	0.032	0.003	1.92×10^{-7}
19	A	Sp	0.035	0.04	0.037	0.035	0.20	0.248	7319	0.003	0.041	0.006	7.8×10^{-7}
20	A	Sp	0.035	0.04	0.037	0.03	0.20	0.241	7319	0.037	0.146	0.06	3.24×10^{-4}
21	A	Sp	0.035	0.04	0.037	0.025	0.20	0.233	7319	0.038	0.158	0.063	3.78×10^{-4}
22	A	Sp	0.035	0.04	0.037	0.02	0.20	0.224	7319	0.035	0.139	0.059	2.87×10^{-4}
23	A	P	0.032	0.045	0.036	0.14	0.20	0.306	7170	0.004[a]	0.109[a]	0.048[a]	2.09×10^{-5}
24	A	P	0.032	0.045	0.036	0.12	0.20	0.3	7170	0.007[a]	0.108[a]	0.06[a]	4.54×10^{-5}
25	A	P	0.032	0.045	0.036	0.10	0.20	0.292	7170	0.005[a]	0.116[a]	0.068[a]	3.94×10^{-5}
26	A	P	0.032	0.045	0.036	0.08	0.20	0.283	7170	0.007[a]	0.126[a]	0.071[a]	$6{,}26 \times 10^{-5}$
27	A	P	0.032	0.045	0.036	0.06	0.20	0.27	7170	0.012[a]	0.163[a]	0.105[a]	2.05×10^{-4}
28	A	P	0.032	0.045	0.036	0.05	0.20	0.263	7170	0.01[a]	0.164[a]	0.12[a]	1.97×10^{-4}
29	A	P	0.032	0.045	0.036	0.04	0.20	0.253	7170	0.014[a]	0.181[a]	0.134[a]	3.4×10^{-4}
30	A	P	0.032	0.045	0.036	0.035	0.20	0.248	7170	0.026[a]	0.267[a]	0.223[a]	1.55×10^{-3}
31	A	P	0.032	0.045	0.036	0.03	0.20	0.241	7170	0.024[a]	0.3[a]	0.248[a]	1.79×10^{-3}
32	A	P	0.032	0.045	0.036	0.025	0.20	0.233	7170	0.004[a]	0.104[a]	0.05[a]	2.08×10^{-5}
33	A	P	0.032	0.045	0.036	0.02	0.20	0.224	7170	0.017[a]	0.201[a]	0.13[a]	4.44×10^{-4}
34	B	C	0.035	0.04	0.037	0.14	0.22	0.306	8050	0.034	0.148	0.063	3.17×10^{-4}
35	B	C	0.035	0.04	0.037	0.12	0.215	0.3	7868	0.034	0.145	0.065	3.20×10^{-4}
36	B	C	0.035	0.04	0.037	0.10	0.21	0.292	7685	0.034	0.145	0.062	3.06×10^{-4}
37	B	C	0.035	0.04	0.037	0.08	0.205	0.283	7502	0.034	0.145	0.065	3.20×10^{-4}
38	B	C	0.035	0.04	0.037	0.06	0.195	0.27	7136	0.034	0.142	0.064	3.09×10^{-4}
39	B	C	0.035	0.04	0.037	0.05	0.19	0.263	6953	0.041	0.178	0.077	5.62×10^{-4}
40	B	C	0.035	0.04	0.037	0.04	0.183	0.253	6697	0.044	0.178	0.077	6.03×10^{-4}
41	B	C	0.035	0.04	0.037	0.035	0.179	0.248	6550	0.047	0.185	0.078	6.78×10^{-4}
42	B	C	0.035	0.04	0.037	0.03	0.173	0.241	6331	0.042	0.176	0.078	5.77×10^{-4}
43	B	C	0.035	0.04	0.037	0.025	0.168	0.233	6148	0.041	0.169	0.077	5.34×10^{-4}
44	B	C	0.035	0.04	0.037	0.02	0.162	0.224	5928	0.037	0.158	0.064	3.74×10^{-4}

C = cube, Sp = sphere, P = pebble. Values are in m, m s^{-1} and m^3. U_c is estimated from Equations (13) and (14).
[a] Indicates scour holes in the wake.

Impact of submergence ratio (d_w/L_o) on obstacle mark formation

The submergence ratio is classified based on disturbances of the water surface profile due to the presence of the obstacle (e.g. Shamloo *et al.*, 2001). At fully submerged conditions ($d_w/L_o > 2$), no disturbance of the water surface profile could be observed, indicating a free flow of the approaching boundary layer above the obstacle top. At shallow submerged conditions ($1 < d_w/L_o < 2$) the obstacle top was only slightly below the water surface, causing the water level to drop above the obstacle top. In addition, a bow wave piles up at the obstacle front. During unsubmerged conditions ($0 < d_w/L_o < 1$), the obstacle top was above the water surface and also a bow wave at the obstacle front could be detected, while in mid to far wake, irregularities of the water surface indicate the presence of trailing vortices due to detached shear layers. The disturbances of the water surface profiles were similar at the different obstacle shapes and for both experimental series (cf. Figure 6).

For series A experiments the typical obstacle mark pattern controlled by the action of the HSV developed at the bluff cuboid obstruction ($Sh \geq 0.8$) for all ratios of d_w/L_o, while this was not applicable for the spherical obstacle ($Sh \leq 0.4$) and the streamlined pebble ($Sh \leq 0.4$) (cf. next section). Concerning the typical obstacle mark morphology, the morphometric variables d_s, w_s and l_s and the normalized scour hole volume ($Vol_s^{1/3}/L_o$) are maximized at $d_w/L_o = 0.8$ to 1.0 (experimental runs A8, A9 and A21). An increase or decrease in d_w/L_o from this threshold causes a limitation of $Vol_s^{1/3}/L_o$ (Figure 7A). At the threshold condition d_w is comparable to L_o, thus a high vertical pressure gradient is present at the obstacle front, creating an intensive downflow and efficient HSV system at the obstacle base. At the threshold condition the secondary control parameter U_m/U_c was 0.83 and 0.81, respectively. Remarkably, although U_m/U_c was higher at unsubmerged conditions (i.e. $U_m/U_c = 0.86$ and 0.89 at $d_w/L_o = 0.68$ and 0.55), $Vol_s^{1/3}/L_o$ is reduced compared to the observed maximum at shallow submerged conditions ($1 < d_w/L_o < 2$), indicating that within the range of constant primary

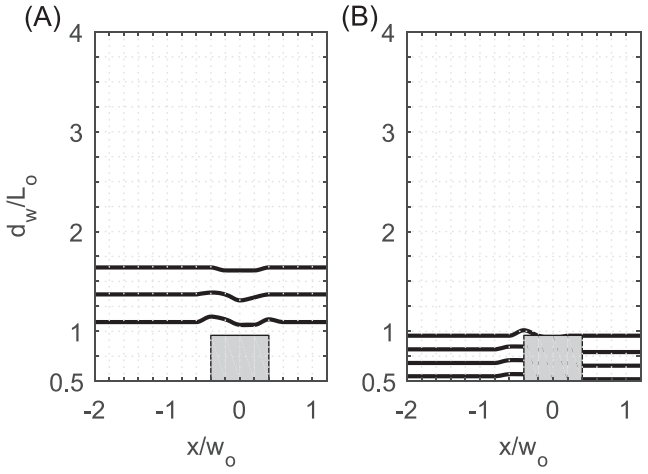

Figure 6. Water surface profiles for series A experiments at a cuboid obstacle. (A) Shallow submerged conditions ($1 < d_w/L_o < 2$). (B) Unsubmerged conditions ($0 > d_w/L_o < 1$). For fully submerged conditions ($d_w/L_o > 2$) no disturbances of the water surface could be detected. Flow direction is from left to right. Punctual measurements are interpolated by piecewise cubic hermite interpolating polynomial.

control parameters ($L_o/D_{50} = 66.5$, $L_o/B = 0.11$), the maximum size of the obstacle mark is determined by d_w/L_o solely. A significant limitation of $Vol_s^{1/3}/L_o$ is also evident for $d_w/L_o > 1.1$ ($U_m/U_c = 0.79$) up to the experimental limit of $d_w/L_o = 3.83$ ($U_m/U_c = 0.65$). The limitation of $Vol_s^{1/3}/L_o$ for both cases can be explained as follows.

(a) for $d_w/L_o < 0.7$, boulder-like obstacles are exposed to a rather shallow flow (i.e. horizontal length scale of flow > vertical scale of flow). For this unsubmerged condition the formation of a bow wave at the obstacle front is observed (cf. Figure 6B). The bow wave interferes with the HSV due to opposite rotation direction (cf. Melville and Coleman, 2000), which limits the spatial extent of the HSV. For $d_w/L_o = 0.55$, obstacle mark formation could be observed in the present investigation. Unfortunately, $d_w/L_o < 0.55$ could not be physically modelled in the laboratory facility. Thus, the threshold of d_w/L_o where the HSV ceases to persist due to the interference of the bow wave could not be detected.

(b) for $d_w/L_o > 1.1$ rising flow depth at the boulder-like obstructions results in a weakening of the vertical pressure gradient in front of the obstacle and eases downflow at the obstacle front. As a consequence, a smaller HSV prevails, because much of the approaching current flows over the obstacle top. The weaker downflow and HSV system damp the incision of d_s and the enlargement of w_s and l_s. Thus, $Vol_s^{1/3}/L_o$ at fully submerged conditions ($d_w/L_o > 2$) is 60% smaller than maximum $Vol_s^{1/3}/L_o$ at $d_w/L_o = 0.8$–1.

The observed threshold condition for maximized $Vol_s^{1/3}/L_o$ at $d_w/L_o \sim 1$ could be validated by series B experiments on the bluff cuboid obstacle ($Sh \geq 0.8$). The actual value of $Vol_s^{1/3}/L_o$ is slightly smaller than for series A experiments, because $U_m/U_c = 0.72$ ($U_m/U_c = 0.81$ at $d_w/L_o \sim 1$ for series A experiments). Moreover, the trend of decreasing $Vol_s^{1/3}/L_o$ compared to the observed maximum is obvious for an increase or decrease of d_w/L_o, which is equivalent to observations of series A experiments (cf. Figure 7B). Remarkably, $Vol_s^{1/3}/L_o$ is fairly constant for experimental runs B34–B38 ($d_w/L_o > 1.6$, $U_m/U_c = 0.72$, $Re_o = 7136$ at $d_w/L_o = 1.64$ to $Re_o = 8050$ at $d_w/L_o = 3.83$). By comparing $Vol_s^{1/3}/L_o$ at different d_w/L_o for both experimental series, it becomes obvious that the assumptions of the parameter framework are accurate. Thus, irrespective of the obstacle shape (Sh), the occurrence of the maximum $Vol_s^{1/3}/L_o$ is solely

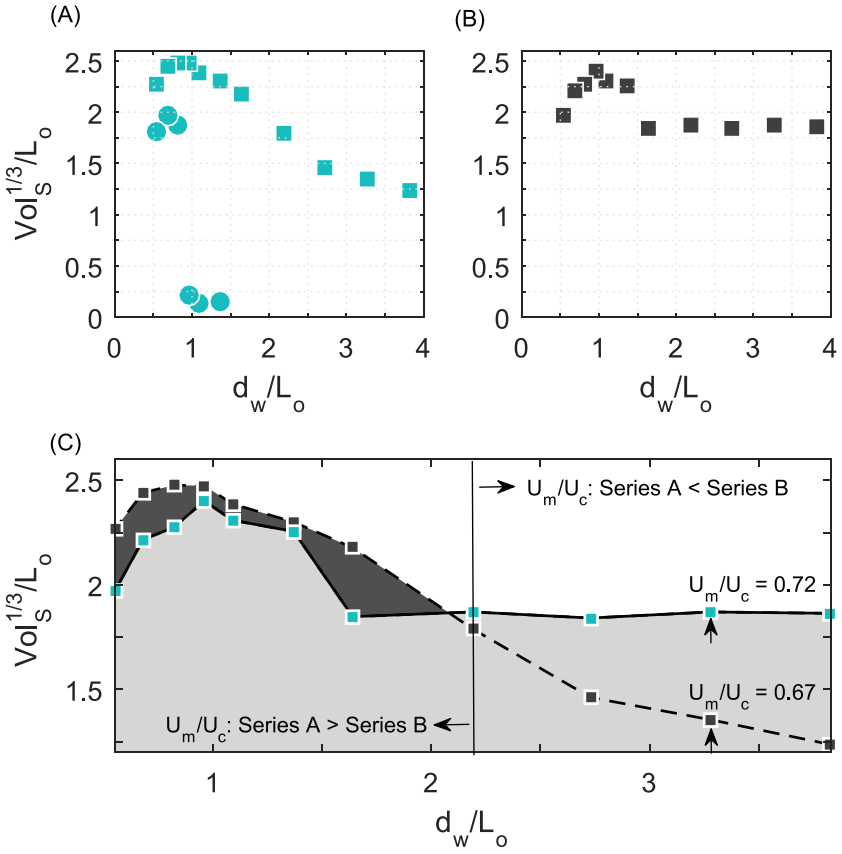

Figure 7. (A) Normalized scour volumes ($Vol_s^{1/3}/L_o$) of runs A1–A11 and A17–A22. Squares = cuboid obstacle, circles = spherical obstacle. (B) Normalized scour volumes ($Vol_s^{1/3}/L_o$) of runs B34–B44. (C) Comparison of (A) and (B) for different d_w/L_o and U_m/U_c. The indications of $U_m/U_c = 0.72$ and $U_m/U_c = 0.67$ are valid for the data point marked by the vertical arrows. [Colour figure can be viewed at wileyonlinelibrary.com]

dependent on the primary control parameter d_w/L_o, while the secondary control parameters U_m/U_c and Re_o impact the actual value of $Vol_s^{1/3}/L_o$ as envelopes to this trend (cf. Figure 7C). Due to restrictions of the laboratory facility, it was not possible to physically model conditions of $d_w/L_o > 3.83$. Thus, thresholds at which local scouring at the bluff angular obstruction ($Sh \geq 0.8$) is completely inhibited could not be determined.

Impact of obstacle shape (C_d) on obstacle mark formation

For the spherical obstacle ($Sh \leq 0.6$), $Vol_s^{1/3}/L_o$ is maximized for unsubmerged conditions at $d_w/L_o \approx 0.7$ (run A21, cf. Figure 8 A), while $Vol_s^{1/3}/L_o$ is 20% less than for the bluff angular obstruction (cf. Figure 7A). Remarkably, an increase in d_w/L_o towards shallow submergence ($1 < d_w/L_o < 2$) emerged as a different morphology of the obstacle mark. Contrary to the typical obstacle mark morphology, the sedimentary structure is then composed of a minor frontal scour hole and two lateral depressions in the wake (runs A17–A19; cf. Figure 8B). For $d_w/L_o > 1.6$, an 'inverse' obstacle mark prevailed at the spherical obstacle ($Sh \leq 0.6$) that is composed of two lateral depressions in the wake and adjacent sediment ridge, while a frontal scour hole is absent (cf. Figure 8C). The morphology of an inverse obstacle mark prevailed for the elliptical obstacle ($Sh \leq 0.4$, runs A23–A33) irrespective of d_w/L_o, while the dimensions of the downstream depression (depth, width and length) decreased with rising d_w/L_o.

At fully submerged conditions ($d_w/L_o = 3.28$), the flow field at the spherical and elliptical obstructions revealed insignificant downflow due to a weak vertical pressure gradient at the obstacle front. Vice versa, the HSV at the base is relatively small in its size, actually smaller than the measuring grid of the ADV measurements (i.e. 0.01 m in the horizontal direction and 0.005 m in the vertical direction) (cf. Truelsen *et al.*, 2005). In the near-wake region, recirculation of approaching flow was present, which is responsible for the observed wake scouring due to turbulence-induced high shear stresses (cf. Figure 9).

Conclusions and Perspectives

Boundary condition control of obstacle mark formation at natural instream obstructions (solitary boulders and vegetation elements) is assessed by a novel parameter framework that incorporates the large body of knowledge derived from hydraulic engineering on local scouring at technical infrastructure (e.g. bridge piers, abutments and pipelines). In total, 13 non-dimensional and scale-invariant control parameters are identified that impact morphodynamic processes at natural instream obstructions. Control parameters are integrated into a systematization that classifies their significance for size of morphometric variables of an obstacle mark based on two hierarchical levels. Seven primary control parameters control the geometrical scale of the turbulent HSV at the obstacle and determine the potential maximum size of the structure, while six secondary control parameters impact the dynamics of the HSV within the geometrical scale and characterize sensitivities of obstacle mark formation. Both hierarchical levels are based on empirical thresholds that are partially derived from an interdisciplinary review on the phenomenon of local scouring at artificial instream obstructions. The purpose of the framework is to identify conditions at which the morphometric variables are maximized, conditions at which morphometric variables are limited compared to the maximum stage and conditions at which the formation of obstacle marks is completely inhibited.

To underpin the proposed classification with an empirical base and to determine threshold conditions of the primary control parameters submergence ratio (d_w/L_o) and obstacle shape (Sh) at which morphometric variables are maximized, two series of small-scale flume experiments were conducted. The submergence ratio (d_w/L_o) was modelled by varying the flow depth (d_w) at obstacles of nearly identical size (L_o) but different

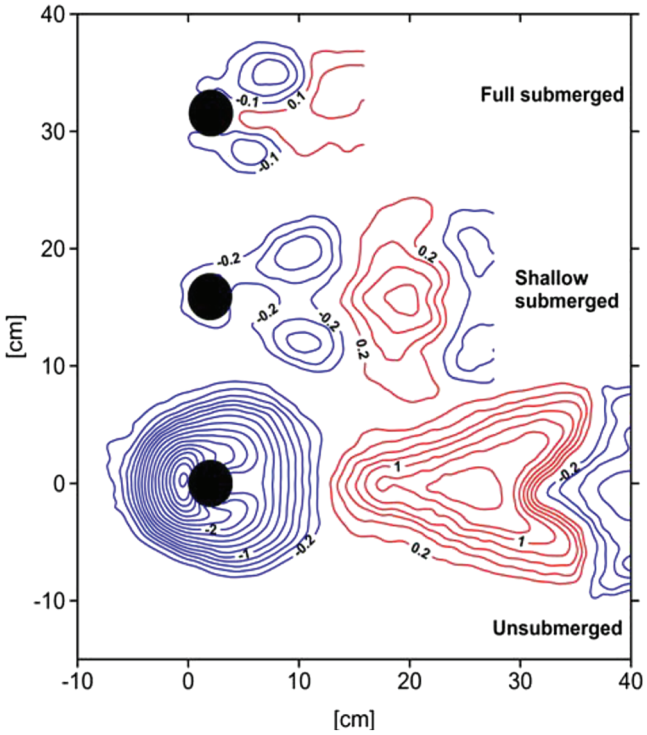

Figure 8. Obstacle mark topography at a spherical obstacle after 24 h runtime for different submergence ratios (d_w/L_o). (A) Inverse obstacle mark. (B) Transitional obstacle mark. (C) Typical obstacle mark. Flow direction from left to right. [Colour figure can be viewed at wileyonlinelibrary.com]

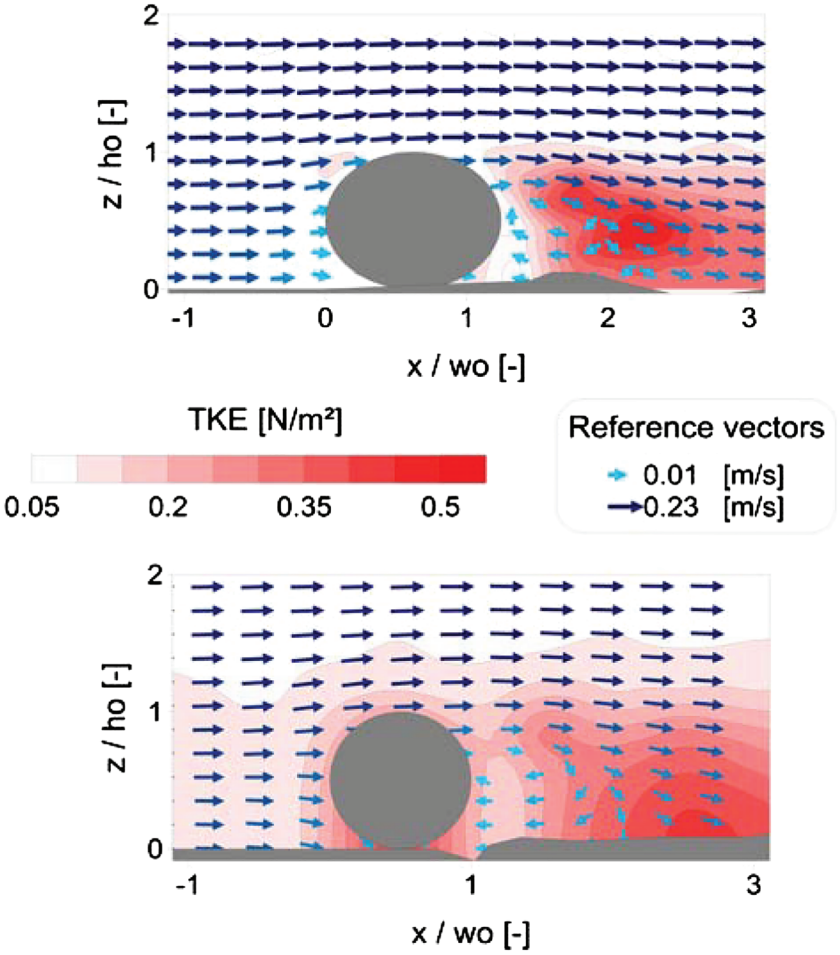

Figure 9. Flow field in the vicinity of (A) elliptical pebble and (B) spherical obstacle for runs A13 and A24. TKE = turbulent kinetic energy (N m^{-2}). Estimate of critical bed shear stress for the sediment used is 0.20 N m^{-2}. [Colour figure can be viewed at wileyonlinelibrary.com]

shape (angular, spherical, elliptical), while the secondary control parameters U_m/U_c and Re_o were also slightly varied.

The normalized scour hole volume ($Vol_s^{1/3}/L_o$) in a near-equilibrium condition (after 24 h) is maximized at angular ($Sh \geq 0.8$) and spherical obstacles ($Sh \leq 0.6$), if d_w is nearly equal to L_o at $d_w/L_o = 0.8$–1.0, while $Vol_s^{1/3}/L_o$ on average is 20% larger for $Sh \geq 0.8$, irrespective of d_w/L_o. For $d_w/L_o = 0.8$–1, a high-pressure gradient exists at the obstacle frontal face and a large HSV prevails at the obstacle base, while an increase or decrease in d_w/L_o from this threshold condition limits the spatial extent of the HSV and vice versa $Vol_s^{1/3}/L_o$. At the spherical obstacle ($Sh \leq 0.6$) no typical obstacle mark (frontal scour hole and downstream sediment accumulation) emerged for $d_w/L_o > 1.6$, while the streamlined shape of the elliptical obstacle ($Sh \leq 0.4$) inhibited the formation of an HSV capable of inducing local scouring in front of the obstruction irrespective of d_w/L_o. Furthermore, the observed dependence of $Vol_s^{1/3}/L_o$ on d_w/L_o is also valid for a variation of the secondary control parameters U_m/U_c and Re_o that impact the dynamics of the HSV, representing envelopes to this trend (cf. Figure 7C). The experimental results confirm the classification of the parameter framework.

The validity of the defined threshold ranges has to be tested empirically for more complex scenarios as an approximation to natural conditions at instream obstructions and their impact on obstacle mark formation. Particularly, flume studies aiming to mimic unsteady discharge events and associated variations in d_w/L_o and U_m/U_c over time (t) are needed. Here, physical modelling studies offer the advantage to gradually and systematically vary control parameters to identify cause and effect relationships and quantify sensitivities, assuming scale independency of processes. Besides the purely academic relevance, increasing knowledge on boundary condition control of fluvial obstacle mark formation and dynamics will refine existing approaches for hydraulic interpretation of preserved obstacle marks that can be used to estimate past flood events (Herget *et al.*, 2013).

Acknowledgement——Open access funding enabled and organized by Projekt DEAL. [Correction added on 31 October 2020, after first online publication: Projekt Deal funding statement has been added.]

Data availability statements

Research data are not shared.

Conflict of interest statement

The authors have no conflict of interest to declare.

References

Alexander J, Cooker MJ. 2016. Moving boulders in flash floods and estimating flow conditions using boulders in ancient deposits. *Sedimentology* **63**(6): 1582–1595.

Allen JRL. 1965. Scour marks in snow. *SEPM Journal of Sedimentary Research* **35**: 331–338.

Allen JRL. 1984. *Sedimentary Structures: Their Character and Physical Basis*. Elsevier: Amsterdam.

Baker VR. 1978. Large-scale erosional and depositional features of the Channeld Scabland. In *The Channeld Scabland: A Guide to the Geomorphology of the Columbia Basin, Washington*, Baker VR, Nummedal D (eds). National Aeronautics and Space Administration (NASA): Washington, D.C.; 81–115.

Baker VR, Bunker RC. 1985. Cataclysmic Late Pleistocene flooding from glacial Lake Missoula: a review. *Quaternary Science Reviews* **4**(1): 1–41.

Barenblatt GI. 2003. *Scaling*. Cambridge University Press: Cambridge.

Bauri KP, Sarkar A. 2016. Flow and scour around vertical submerged structures. *Sadhana* **41**(9): 1039–1053.

Biron PM, Robson C, Lapointe MF, Gaskin SJ. 2004. Comparing different methods of bed shear stress estimates in simple and complex flow fields. *Earth Surface Processes and Landforms* **29**(11): 1403–1415.

Bishop MA. 2011. Aeolian scours as putative signatures of wind erosion and sediment transport direction on Mars. *Geomorphology* **125**(4): 569–574.

Bouratsis P, Diplas P, Dancey CL, Apsilidis N. 2017. Quantitative spatio-temporal characterization of scour at the base of a cylinder. *Water* **9**(3): 227. https://doi.org/10.3390/w9030227

Brandimarte L, Montanari A, Briaud J-L, D'Odorico P. 2006. Stochastic flow analysis for predicting river scour of cohesive soils. *Journal of Hydraulic Engineering* **132**(5): 493–500.

Bressan L, Guerrero M, Antonini A, Petruzzelli V, Archetti R, Lamberti A, Tinti S. 2018. A laboratory experiment on the incipient motion of boulders by high-energy coastal flows. *Earth Surface Processes and Landforms* **43**(14): 2935–2947.

Breusers HNC, Raudkivi AJ. 1991. *Scouring*. Balkema: Rotterdam.

Briaud J-L, Ting FCK, Chen HC, Gudavalli R, Perugu S, Wei G. 1999. SRICOS: prediction of scour rate in cohesive soils at bridge piers. *Journal of Geotechnical and Geoenvironmental Engineering* **125**(4): 237–246.

Buffington JM, Lisle TE, Woodsmith RD, Hilton S. 2002. Controls on the size and occurrence of pools in coarse-grained forest rivers. *River Research and Applications* **18**(6): 507–531.

Carling PA, Hoffmann M, Blatter AS. 2002a. Initial motion of boulders in bedrock channels. In *Ancient Floods, Modern Hazards: Principles and Applications of Paleoflood Hydrology*, House PK (ed). American Geophysical Union: Washington, D.C.; 147–160.

Carling PA, Kirkbride AD, Parnachov S, Borodavko PS, Berger GW. 2002b. Late Quaternary catastrophic flooding in the Altai Mountains of south–central Siberia: a synoptic overview and an introduction to flood deposit sedimentology. In *Flood and Megaflood Processes and Deposits: Recent and Ancient Examples*, Garzón G, Martini IP, Baker VR (eds). Blackwell Science: Oxford; 17–35.

Chang W-Y, Lai J-S, Yen C-L. 2004. Evolution of scour depth at circular bridge piers. *Journal of Hydraulic Engineering* **130**(9): 905–913.

Chanson H, Trevethan M, S-i A. 2008. Acoustic Doppler velocimetry (ADV) in small estuary: field experience and signal post-processing. *Flow Measurement and Instrumentation* **19**(5): 307–313.

Chen S-C, Chan H-C, Li Y-H. 2012. Observations on flow and local scour around submerged flexible vegetation. *Advances in Water Resources* **43**: 28–37.

Chiew Y-M. 1995. Mechanics of riprap failure at bridge piers. *Journal of Hydraulic Engineering* **121**(9): 635–643.

Chojnacki M, Banks ME, Fenton LK, Urso AC. 2019. Boundary condition controls on the high-sand-flux regions of Mars. *Geology* **47**(5): 427–430.

Chou JH, Chao SY. 2000. Branching of a horseshoe vortex around surface-mounted rectangular cylinders. *Experiments in Fluids* **28**(5): 394–402.

Chreties C, Simarro G, Teixeira L. 2008. New experimental method to find equilibrium scour at bridge piers. *Journal of Hydraulic Engineering* **134**(10): 1491–1495.

Church M, Haschenburger JK. 2017. What is the "active layer"? *Water Resources Research* **53**(1): 5–10.

Coco G, Murray AB. 2007. Patterns in the sand: from forcing templates to self-organization. *Geomorphology* **91**: 271–290.

Comiti F, Andreoli A, Lenzi MA. 2005. Morphological effects of local scouring in step–pool streams. *Earth Surface Processes and Landforms* **30**(12): 1567–1581.

Corenblit D, Vidal V, Cabanis M, Steiger J, Garófano-Gómez V, Garreau A, Hortobágyi B, Otto T, Roussel E, Voldoire O. 2016. Seed retention by pioneer trees enhances plant diversity resilience on gravel bars: observations from the river Allier, France. *Advances in Water Resources* **93**: 182–192.

Dal CR. 1968. "Pebble clusters": their origin and utilization in the study of paleocurrents. *Sedimentary Geology* **2**(4): 233–241.

Dargahi B. 1989. The turbulent flow field around a circular cylinder. *Experiments in Fluids* **8**(1–2): 1–12.

Dargahi B. 1990. Controlling mechanism of local scouring. *Journal of Hydraulic Engineering* **116**(10): 1197–1214.

Debnath K, Chaudhuri S. 2010. Laboratory experiments on local scour around cylinder for clay and clay–sand mixed beds. *Engineering Geology* **111**(1–4): 51–61.

Dey S. 1996. Sediment pick-up for evolving scour near circular cylinders. *Applied Mathematical Modelling* **20**(7): 534–539.

Dey S. 1999. Time-variation of scour in the vicinity of circular piers. *Proceedings of the Institution of Civil Engineers – Water Maritime and Energy* **136**(2): 67–75.

Dey S, Bose SK, Sastry GLN. 1995. Clear water scour at circular piers: a model. *Journal of Hydraulic Engineering* **121**(12): 869–876.

Dey S, Raikar RV. 2007a. Characteristics of horseshoe vortex in developing scour holes at piers. *Journal of Hydraulic Engineering* **133**(4): 399–413.

Dey S, Raikar RV. 2007b. Clear-water scour at piers in sand beds with an armor layer of gravels. *Journal of Hydraulic Engineering* **133**(6): 703–711.

Dey S, Raikar RV, Roy A. 2008. Scour at submerged cylindrical obstacles under steady flow. *Journal of Hydraulic Engineering* **134**(1): 105–109.

Douglas JF, Gasiorek JM, Swaffield JA. 2001. *Fluid Mechanics*. Harlow: Prentice Hall.

Dżułyński S, Walton EK. 1965. *Sedimentary Features of Flysch and Greywackes*. Elsevier: Amsterdam.

Endreny T, Lautz L, Siegel DI. 2011. Hyporheic flow path response to hydraulic jumps at river steps: flume and hydrodynamic models. *Water Resources Research* **47**(2): W02517. https://doi.org/10.1029/2009WR008631

Ettema R, Constantinescu G, Melville BW. 2011. *Evaluation of Bridge Scour Research: Pier Scour Processes and Predictions*. Transportation Research Board: Washington, D.C.

Ettema R, Kirkil G, Muste M. 2006. Similitude of large-scale turbulence in experiments on local scour at cylinders. *Journal of Hydraulic Engineering* **132**(1): 33–40.

Ettema R, Melville BW, Barkdoll B. 1998. Scale effect in pier-scour experiments. *Journal of Hydraulic Engineering* **124**(6): 639–642.

Euler T, Herget J. 2011. Obstacle-Reynolds-number based analysis of local scour at submerged cylinders. *Journal of Hydraulic Research* **49**(2): 267–271.

Euler T, Herget J. 2012. Controls on local scour and deposition induced by obstacles in fluvial environments. *CATENA* **91**: 35–46.

Euler T, Herget J, Schlömer O, Benito G. 2017. Hydromorphological processes at submerged solitary boulder obstacles in streams. *CATENA* **157**: 250–267.

Euler T, Zemke J, Rodrigues S, Herget J. 2014. Influence of inclination and permeability of solitary woody riparian plants on local hydraulic and sedimentary processes. *Hydrological Processes* **28**(3): 1358–1371.

Ewing RC, Kocurek G. 2010. Aeolian dune-field pattern boundary conditions. *Geomorphology* **114**(3): 175–187.

Filhol S, Sturm M. 2015. Snow bedforms: a review, new data, and a formation model. *Journal of Geophysical Research: Earth Surface* **120**(9): 1645–1669.

Firat M, Gungor M. 2009. Generalized regression neural networks and feed forward neural networks for prediction of scour depth around bridge piers. *Advances in Engineering Software* **40**(8): 731–737.

Fisher AC, Klingeman PC. 1984. Local scour at fish rocks. In *Water for Resource Development: Proceedings of the Conference of the American Society of Civil Engineers, Coeur d'Alene, ID, 14–17 August*, Schreiber DL (ed). ASCE: New York; 286–290.

Friedrich CT, Rennie SE, Brandt A. 2016. Self-burial of objects on sandy bed by scour: a synthesis of observations. In *Scour and Erosion: Proceedings of the 8th International Conference on Scour and Erosion, Oxford, UK, 12–15 September*, Harris J, Whitehouse R, Moxon S (eds). CRC Press: Boca Raton, FL; 179–189.

Garlan T, Marches E, Brenon E. 2015. A classification of scouring marks in macrotidal environments from analysis of long term wreck marks. In *The Proceedings of the Coastal Sediments 2015*, Wang P, Rosati JD, Cheng J (eds). World Scientific: Singapore; 14.

Ghilardi T, Franca MJ, Schleiss AJ. 2014a. Bed load fluctuations in a steep channel. *Water Resources Research* **50**(8): 6557–6576.

Ghilardi T, Franca MJ, Schleiss AJ. 2014b. Period and amplitude of bedload pulses in a macro-rough channel. *Geomorphology* **221**: 95–103.

Goring DG, Nikora VI. 2002. Despiking acoustic Doppler velocimeter data. *Journal of Hydraulic Engineering* **128**(1): 117–126.

Grant PF, Nickling WG. 1998. Direct field measurement of wind drag on vegetation for application to windbreak design and modelling. *Land Degradation & Development* **9**(1): 57–66.

Hajimirzaie SM, Tsakiris AG, Buchholz JHJ, Papanicolaou AN. 2014. Flow characteristics around a wall-mounted spherical obstacle in a thin boundary layer. *Experiments in Fluids* **55**(6): 1762. https://doi.org/10.1007/s00348-014-1762-0

Hassan MA, Woodsmith RD. 2004. Bed load transport in an obstruction-formed pool in a forest, gravelbed stream. *Geomorphology* **58**(1–4): 203–221.

Herget J. 2005. *Reconstruction of Pleistocene Ice-Dammed Lake Outburst Floods in the Altai Mountains, Siberia*. Boulder, CO.: Geological Society of America.

Herget J, Euler T, Roggenkamp T, Zemke J. 2013. Obstacle marks as palaeohydraulic indicators of Pleistocene megafloods. *Hydrology Research* **44**(2): 300–317.

Hodge RA, Hoey TB, Sklar LS. 2011. Bed load transport in bedrock rivers: the role of sediment cover in grain entrainment, translation, and deposition. *Journal of Geophysical Research* **116**: F04028. https://doi.org/10.1029/2011JF002032

Hoffmans GJCM. 1993. A hydraulic and morphological criterion of upstream slopes in local scour holes. In *Report W-DWW-93-255*. Delft: Rijkswaterstaat.

Hoffmans GJCM, Verheij HJ. 1997. *Scour Manual*. Balkema: Rotterdam.

Høgaas F, Longva O. 2016. Mega deposits and erosive features related to the glacial lake Nedre Glomsjø outburst flood, southeastern Norway. *Quaternary Science Reviews* **151**: 273–291.

Hong J-H, Chiew Y-M, Yeh P-H, Chan H-C. 2017. Evolution of local pier-scour depth with dune migration in subcritical flow conditions. *Journal of Hydraulic Engineering* **143**(4): 4016098. https://doi.org/10.1061/(ASCE)HY.1943-7900.0001261

Judd HE, Peterson DF. 1969. Hydraulics of large bed element channels. In *Report PRWG 17-6*. Logan, UT: Utah Water Research Laboratory.

Karcz I. 1968. Fluviatile obstacle marks from the wadis of the Negev (southern Israel). *SEPM Journal of Sedimentary Research* **38**: 1000–1012.

Kim HS, Kimura I, Shimizu Y. 2015. Bed morphological changes around a finite patch of vegetation. *Earth Surface Processes and Landforms* **40**(3): 375–388.

Kim S-C, Friedrichs CT, Maa JP-Y, Wright LD. 2000. Estimating bottom stress in tidal boundary layer from acoustic Doppler velocimeter data. *Journal of Hydraulic Engineering* **126**(6): 399–406.

Kocurek G, Ewing RC, Mohrig D. 2010. How do bedform patterns arise? New views on the role of bedform interactions within a set of boundary conditions. *Earth Surface Processes and Landforms* **35**(1): 51–63.

Kothyari UC, Garde RCJ, Ranga Raju KG. 1992. Temporal variation of scour around circular bridge piers. *Journal of Hydraulic Engineering* **118**(8): 1091–1106.

Kramer CM, Papanicolaou AN. 2006. The effects of relative submergence on flow patterns around large particles in a gravel bed river. In *Examining the Confluence of Environmental and Water Concerns: Proceedings of the 2006 World Environmental and Water Resources Congress, Omaha, NE, 21–25 May*, Graham R (ed). American Society of Civil Engineers: Reston, VA; 1–10.

Lacey RWJ, Rennie CD. 2012. Laboratory investigation of turbulent flow structure around a bed-mounted cube at multiple flow stages. *Journal of Hydraulic Engineering* **138**(1): 71–84.

Lança RM, Simarro G, Fael SCM, Cardoso AH. 2016. Effect of viscosity on the equilibrium scour depth at single cylindrical piers. *Journal of Hydraulic Engineering* **142**(3): 6015022. https://doi.org/10.1061/(ASCE)HY.1943-7900.0001102

Laronne JB, Garcia C, Reid I. 2001. Mobility of patch sediment in gravel bed streams: patch character and its implications for bedload. In *Gravel-Bed Rivers*, Mosley MP (ed). New Zealand Hydrological Society: Wellington; 249–289.

Launay G, Mignot E, Riviere N, Perkins R. 2017. An experimental investigation of the laminar horseshoe vortex around an emerging obstacle. *Journal of Fluid Mechanics* **830**: 257–299.

Lee C, Kim D, Kim S, Ji U, Dongwoo K. 2018. Flow structure around an actual willow patch under different depth conditions. *E3S Web of Conferences* **40**(1): 02049.

Lee SO, Sturm TW. 2009. Effect of sediment size scaling on physical modeling of bridge pier scour. *Journal of Hydraulic Engineering* **135**(10): 793–802.

Leenders JK, van Boxel JH, Sterk G. 2007. The effect of single vegetation elements on wind speed and sediment transport in the Sahelian zone of Burkina Faso. *Earth Surface Processes and Landforms* **32**(10): 1454–1474.

Li J, Qi M, Fuhrman DR, Chen Q. 2018. Influence of turbulent horseshoe vortex and associated bed shear stress on sediment transport in front of a cylinder. *Experimental Thermal and Fluid Science* **97**: 444–457.

Link O, González C, Maldonado M, Escauriaza C. 2012. Coherent structure dynamics and sediment particle motion around a cylindrical pier in developing scour holes. *Acta Geophysica* **60**(6): 1689–1719.

Link O, Pfleger F, Zanke U. 2008. Characteristics of developing scourholes at a sand-embedded cylinder. *International Journal of Sediment Research* **23**(3): 258–266.

Lisle TE. 1981. Roughness elements: a key resource to improve anadromous fish habitat. In *Proceedings of the Propagation, Enhancement and Rehabilitation of Anadromous Salmonid Populations and Habitat in the Pacific Northwest Symposium*, Hassler TJ (ed). Humboldt State University: Arcata; 93–98.

Luo W, Dong Z, Qian G, Lu J. 2012. Wind tunnel simulation of the three-dimensional airflow patterns behind cuboid obstacles at different angles of wind incidence, and their significance for the formation of sand shadows. *Geomorphology* **139–140**: 258–270.

Maity H, Mazumder BS. 2014. Experimental investigation of the impacts of coherent flow structures upon turbulence properties in regions of crescentic scour. *Earth Surface Processes and Landforms* **39**(8): 995–1013.

Manes C, Brocchini M. 2015. Local scour around structures and the phenomenology of turbulence. *Journal of Fluid Mechanics* **779**: 309–324.

Manes C, Coscarella F, Rogers A, Gaudio R, Paquier A, Rivière N. 2018. Viscosity effects on local scour around vertical structures in clear-water conditions. *E3S Web of Conferences* **40**(1): 3038. https://doi.org/10.1051/e3sconf/20184003038

Mazumder BS, Maity H, Chadda T. 2011. Turbulent flow field over fluvial obstacle marks generated in a laboratory flume. *International Journal of Sediment Research* **26**(1): 62–77.

McKenna Neuman C, Sanderson RS, Sutton S. 2013. Vortex shedding and morphodynamic response of bed surfaces containing non-erodible roughness elements. *Geomorphology* **198**: 45–56.

Melville BW, Chiew Y-M. 1999. Time scale for local scour at bridge piers. *Journal of Hydraulic Engineering* **125**(1): 59–65.

Melville BW, Coleman SE. 2000. *Bridge Scour*. Highlands Ranch, CO.: Water Resources Publications.

Melville BW, Sutherland AJ. 1988. Design method for local scour at bridge piers. *Journal of Hydraulic Engineering* **114**(10): 1210–1226.

Mia MF, Nago H. 2003. Design method of time-dependent local scour at circular bridge pier. *Journal of Hydraulic Engineering* **129**(6): 420–427.

Montakhab A, bt.Yusuf B, Ghazali AH, Mohamed TA. 2013. Estimation of vegetation porosity in vegetated waterways. *Proceedings of the Institution of Civil Engineers – Water Management* **166**(6): 333–340.

Murray AB, Coco G, Goldstein EB. 2014. Cause and effect in geomorphic systems: complex systems perspectives. *Geomorphology* **214**: 1–9.

Muste M (ed). 2017. *Experimental Hydraulics: Methods, Instrumentation. Data Processing and Management*. CRC Press: Boca Raton, FL.

Muzzammil M, Gangadharaiah T, Gupta AK. 2004. An experimental investigation of a horseshoe vortex induced by a bridge pier. *Proceedings of the Institution of Civil Engineers – Water Management* **157**(2): 109–119.

Muzzammil M, Gangadhariah T. 2003. The mean characteristics of horseshoe vortex at a cylindrical pier. *Journal of Hydraulic Research* **41**(3): 285–297.

Nakayama K. 1992. Fluvial gravel beds with superimposed boulders in the Seto Group, Japan. *Journal of Sedimentological Society of Japan* **37**(3): 79–84.

Nakayama K, Fielding CR, Alexander J. 2002. Variations in character and preservation potential of vegetation-induced obstacle marks in the variable discharge Burdekin River of north Queensland, Australia. *Sedimentary Geology* **149**(4): 199–218.

Nezu I, Nakagawa H. 1993. *Turbulence in Open-Channel Flows*. Balkema: Rotterdam.

Nikora V. 2010. Hydrodynamics of aquatic ecosystems: an interface between ecology, biomechanics and environmental fluid mechanics. *River Research and Applications* **26**(4): 367–384.

Nikora V, Larned S, Nikora N, Debnath K, Cooper G, Reid M. 2008. Hydraulic resistance due to aquatic vegetation in small streams: field study. *Journal of Hydraulic Engineering* **134**(9): 1326–1332.

Okamoto T, Nezu I. 2010. Flow resistance law in open channel flows with rigid and flexible vegetation. In *River Flow 2010: Proceedings of the 5th International Conference on Fluvial Hydraulics, Braunschweig, Germany, 8–10 June 2010*, Dittrich A (ed). Bundesanst. für Wasserbau: Karlsruhe; 261–268.

Oliveto G, Hager WH. 2002. Temporal evolution of clear-water pier and abutment scour. *Journal of Hydraulic Engineering* **128**(9): 811–820.

Oliveto G, Hager WH. 2014. Morphological evolution of dune-like bed forms generated by bridge scour. *Journal of Hydraulic Engineering* **140**(5): 6014009. https://doi.org/10.1061/(ASCE)HY.1943-7900.0000853

Pagliara S, Palermo M, Paquier A, Rivière N. 2018. Equilibrium scour morphology downstream of rock sills under unsteady flow conditions. *E3S Web of Conferences* **40**: 3004. https://doi.org/10.1051/e3sconf/20184003004

Paola C, Gust G, Southard J. 1986. Skin friction behind isolated hemispheres and the formation of obstacle marks. *Sedimentology* **33**(2): 279–293.

Strom KB, Papanicolaou AN. 2008. Morphological characterization of cluster microforms. *Sedimentology* **55**(1): 137–153.

Papanicolaou AN, Dermisis DC, Elhakeem M. 2011. Investigating the role of clasts on the movement of sand in gravel bed rivers. *Journal of Hydraulic Engineering* **137**(9): 871–883.

Papanicolaou AN, Kramer C. 2006. Flow and sediment laboratory measurements over unsubmerged roughness elements. In *Examining the Confluence of Environmental and Water Concerns: Proceedings of the 2006 World Environmental and Water Resources Congress, May 21–25, 2006*, Omaha NE, Graham R (eds). American Society of Civil Engineers: Reston, VA; 1–8.

Papanicolaou AN, Kramer CM, Tsakiris AG, Stoesser T, Bomminayuni S, Chen Z. 2012. Effects of a fully submerged boulder within a boulder array on the mean and turbulent flow fields: implications to bedload transport. *Acta Geophysica* **60**(6): 1502–1546.

Papanicolaou AN, Tsakiris AG. 2017. Boulder effects on turbulence and bedload transport. In *Gravel-Bed Rivers*, Tsutsumi D, Laronne JB (eds). Wiley: Chichester; 33–72.

Papanicolaou AN, Tsakiris AG, Kramer CM. 2010. Effects of relative submergence on flow and sediment patterns around clasts. In *River Flow 2010: Proceedings of the 5th International Conference on Fluvial Hydraulics, Braunschweig, Germany, 8–10 June 2010*, Dittrich A (ed). Bundesanst. für Wasserbau: Karlsruhe; 793–799.

Papanicolaou AN, Tsakiris AG, Wyssmann MA, Kramer CM. 2018. Boulder array effects on bedload pulses and depositional patches. *Journal of Geophysical Research: Earth Surface* **123**(11): 2925–2953.

Pattenden RJ, Turnock SR, Zhang X. 2005. Measurements of the flow over a low-aspect-ratio cylinder mounted on a ground plane. *Experiments in Fluids* **39**(1): 10–21.

Peabody FE. 1947. Current crescents in the Triassic Moenkopi Formation [Arizona]. *SEPM Journal of Sedimentary Research* **17**(2): 73–76.

Poesen JW, Torri D, Bunte K. 1994. Effects of rock fragments on soil erosion by water at different spatial scales: a review. *CATENA* **23**(1–2): 141–166.

Quinn R. 2006. The role of scour in shipwreck site formation processes and the preservation of wreck-associated scour signatures in the sedimentary record – evidence from seabed and sub-surface data. *Journal of Archaeological Science* **33**(10): 1419–1432.

Quinn R, Smyth TAG. 2017. Processes and patterns of flow, erosion, and deposition at shipwreck sites: a computational fluid dynamic simulation. *Archaeological and Anthropological Sciences* **10**(6):1429–1442

Radice A, Porta G, Franzetti S. 2009. Analysis of the time-averaged properties of sediment motion in a local scour process. *Water Resources Research* **45**(3): 1069–1081.

Radspinner RR, Diplas P, Lightbody AF, Sotiropoulos F. 2010. River training and ecological enhancement potential using in-stream structures. *Journal of Hydraulic Engineering* **136**(12): 967–980.

Raudkivi AJ, Ettema R. 1985. Scour at cylindrical bridge piers in armored beds. *Journal of Hydraulic Engineering* **111**(4): 713–731.

Rennie SE, Brandt A, Friedrichs CT. 2017. Initiation of motion and scour burial of objects underwater. *Ocean Engineering* **131**: 282–294.

Richardson K, Carling PA. 2005. A typology of sculpted forms in open bedrock channels. In *In Special Paper 392: A typology of sculpted forms in open bedrock channels*. Boulder, CO.: Geological Society of America.

Richardson PD. 1968. The generation of scour marks near obstacles. *SEPM Journal of Sedimentary Research* **38**(4): 965–970.

Rodrigues S, Bréhéret J-G, Macaire J-J, Greulich S, Villar M. 2007. In-channel woody vegetation controls on sedimentary processes and the sedimentary record within alluvial environments: a modern example of an anabranch of the River Loire, France. *Sedimentology* **54**(1): 223–242.

Russell AJ. 1993. Obstacle marks produced by flow around stranded ice blocks during a glacier outburst flood (jokulhlaup) in west Greenland. *Sedimentology* **40**(6): 1091–1111.

Russell AJ, Roberts MJ, Fay H, Marren PM, Cassidy NJ, Tweed FS, Harris T. 2006. Icelandic jökulhlaup impacts: implications for ice-sheet hydrology, sediment transfer and geomorphology. *Geomorphology* **75**(1–2): 33–64.

Rygel MC, Gibling MR, Calder JH. 2004. Vegetation-induced sedimentary structures from fossil forests in the Pennsylvanian Joggins Formation, Nova Scotia. *Sedimentology* **51**(3): 531–552.

Sarkar A. 2014. Scour and flow around submerged structures. *Proceedings of the Institution of Civil Engineers – Water Management* **167**(2): 65–78.

Schlömer O, Herget J. 2016. Physical modeling of fluvial obstacle marks at a sediment layer of limited thickness. In *MARID 2016: Fifth International Conference on Marine and River Dune Dynamics, Caernafon, UK, 4–6 April*, Van Landeghem KJJ, Garlan T, Baas JH (eds); 159–162.

Schnauder I, Moggridge HL. 2009. Vegetation and hydraulic–morphological interactions at the individual plant, patch and channel scale. *Aquatic Sciences* **71**(3): 318–330.

Shamloo H, Rajaratnam N, Katopodis C. 2001. Hydraulics of simple habitat structures. *Journal of Hydraulic Research* **39**(4): 351–366.

Sheppard DM, Melville B, Demir H. 2014. Evaluation of existing equations for local scour at bridge piers. *Journal of Hydraulic Engineering* **140**(1): 14–23.

Sheppard DM, Miller W. 2006. Live-bed local pier scour experiments. *Journal of Hydraulic Engineering* **132**(7): 635–642.

Simarro G, Teixeria L, Cardoso AH. 2007. Flow intensity parameter in pier scour experiments. *Journal of Hydraulic Engineering* **133**(11): 1261–1264.

Simons DB, Richardson EV. 1966. *Resistance to flow in alluvial channels*. US Geological Survey Professional Paper 422-J: Washington, D.C.

Sonin AA. 2004. A generalization of the π-theorem and dimensional analysis. *PNAS* **101**(23): 8525–8526.

Sumer BM. 2004. Physical and mathematical modelling of scour. In *Proceedings of the 2nd International Conference on Scour and Erosion (ICSE-2), 14–17 November*, Chiew Y-M, Lim S-Y, Cheng N-S (eds). World Scientific: Singapore; 29–46.

Sumer BM, Fredsøe J. 2005. *The Mechanics of Scour in the Marine Environment*. World Scientific: Hackensack, NJ.

Sumner D. 2013. Flow above the free end of a surface-mounted finite-height circular cylinder: a review. *Journal of Fluids and Structures* **43**: 41–63.

Thompson DM. 2008. The influence of lee sediment behind large bed elements on bedload transport rates in supply-limited channels. *Geomorphology* **99**(1–4): 420–432.

Tominga A. 2014. Flow structure and bed deformation around a sphere on moveable bed. In *River Flow 2014: Proceedings of the International Conference on Fluvial Hydraulics, Lausanne, Switzerland, 3–5 September*, Schleiss AJ, de Cesare G, Franca MJ, Pfister M (eds). CRC Press/Balkema: Boca Raton, FL/Rotterdam; 1499–1507.

Tooth S, Nanson GC. 2000. The role of vegetation in the formation of anabranching channels in an ephemeral river, Northern plains, arid central Australia. *Hydrological Processes* **14**(16–17): 3099–3117.

Truelsen C, Sumer BM, Fredsøe J. 2005. Scour around spherical bodies and self-burial. *Journal of Waterway, Port, Coastal, and Ocean Engineering* **131**(1). https://doi.org/10.1061/(ASCE)0733-950X(2005)131:1(1)

Unger J, Hager WH. 2007. Down-flow and horseshoe vortex characteristics of sediment embedded bridge piers. *Experiments in Fluids* **42**(1): 1–19.

Wahl TL. 2000. Analyzing ADV data using WinADV. In *Building Partnerships*, Hotchkiss RH (ed). American Society of Civil Engineers: Reston, VA; 1–10.

Werner BT. 1999. Complexity in natural landform patterns. *Science* **284**(5411): 102–104.

Werner BT. 2003. Modeling landforms as self-organized, hierarchical dynamical systems. In *Prediction in Geomorphology*, Wilcock PR, Iverson RM (eds). American Geophysical Union: Washington, D.C.; 133–150.

Werner F, Unsöld G, Koopmann B, Stefanon A. 1980. Field observations and flume experiments on the nature of comet marks. *Sedimentary Geology* **26**(1–3): 233–262.

Williams P, Bolisetti T, Balachandar R. 2017. Evaluation of governing parameters on pier scour geometry. *Canadian Journal of Civil Engineering* **44**(1): 48–58.

Wu P, Balachandar R. 2016. Local scour around bridge abutments including effects of relative bed coarseness and blockage ratio. *Canadian Journal of Civil Engineering* **43**(1): 51–59.

Yagci O, Celik MF, Kitsikoudis V, Ozgur Kirca VS, Hodoglu C, Valyrakis M, Duran Z, Kaya S. 2016. Scour patterns around isolated vegetation elements. *Advances in Water Resources* **97**: 251–265.

Yin D, Peakall J, Parsons D, Chen Z, Averill HM, Wignall P, Best J. 2016. Bedform genesis in bedrock substrates: insights into formative processes from a new experimental approach and the importance of suspension-dominated abrasion. *Geomorphology* **255**: 26–38.

